Ref. Ares(2020)7389226 - 07/12/2020

Optimization of scalaBle rEaltime modeLs and functIonal testing for e-drive ConceptS

EUROPEAN COMMISSION

Horizon 2020

GV-07-2017

GA # 769506

Deliverable No.	OBELICS D6.3	
Deliverable Title	Simulation and Test Reports on the Assessment of Safety and Reliability Methods	
Deliverable Date	09/11/2020	
Deliverable Type	REPORT	
Dissemination level	Public (PU)	
Written By	Beyza Atar (FO) Caner Harman (FO) Ahu Ece Hartavi KARCI (US) Mohammad Ghazali (US) Abhishek Shah Alias Sangani (US) Jürgen Nuffer (LBF)	2020/09/09 2020/12/03 2020/11/04 2020/11/04 2020/11/04 2020/12/03
Reviewed by	Benjamin Zillmann(BOSCH) Kazusa Yamamoto (VALEO) Mathieu Sarrazin (SIE)	2020/11/25 2020/11/20 2020/12/03
Approved by	Horst Pfluegl (AVL) – Project Coordinator	2020/12/03
Status	Final	2020/12/03

Change log:

No	Who	Description	Date
1	Mathieu Sarrazin	Initial draft and structure of document	6.12.2019
2	Mathieu Sarrazin	Update draft	23.01.2020
3	Caner Harman	Update Draft	31.05.2020
4	Caner Harman	Update Draft based on WP6 structure	26.06.2020
5	Beyza Atar	UC 3.4 Ford Otosan contribution added.	09.09.2020
6	Marco Ranieri	Added CEA contribution	13.10.2020
7	Caner Harman	Structurally updated	25.10.2020
8	Marco Ranieri	Final corrections of the CEA sections	03-11-2020
9	Abhishek Shah Alias Sangani	Integration of UC3.4 University of Surrey's contribution	04-11-2020
10	Marco Ranieri	Clarification of the safety improvement results (CEA)	17/11/2020
11	Jürgen Nuffer	Implementation of WP5 contribution to safety assessment	18/11/2020
12	Caner Harman	Table 5.2 and appendix tables are updated	03/12/2020

Contents

Figures

Tables

1 Publishable Executive Summary

OBELICS project focusses on the development of a systematic, comprehensive and advanced model-based design and testing framework to support the development of next generation of e-powertrains systems and new EVs lines-up. Overall objective is to reduce development efforts by 40 % while improving efficiency of the e-drivetrain by 20 % and increase safety by a factor of 10 by implementing OBELICS methodologies and tools in a vehicle development process among which advanced virtual integration tools, new heterogeneous model-based testing methods and tools, scalable and easy to parameterize simulations and real time models.

In order to make sure that the objective will be achieved, OBELICS introduces industrial and prospective use cases to apply and prove new methods and tools. Use cases represent typical engineering activities in the development process of e-vehicles. Total of 17 use cases proposed within OBELICS project and they are clustered in 4 groups. One of these clusters is use case cluster 3 where battery design and testing for improved safety reliability studied by total of 8 partners. The battery forms a key component of the electric powertrain. Testing and development of the battery is a time-consuming process and needs about 2 to 5 years from concept to production phase. Accelerating this development process would therefore quicken the production of the vehicle. Adoption of model-based battery development methods reduces the effort and time and consequently increases efficiency of battery production. Deliverable D6.3 contain the major outputs of use case cluster three and focuses on component to vehicle safety and reliability assessment based on simulation and testing methods.

The four considered use cases are UC3.1 *'Battery safety improvement & Testing'*, UC3.2 *'20 kHz battery assessment & Testing technologies'*, UC3.3 *'Battery reliability testing and safety improvement'*, UC3.4 *'Light commercial demonstrator'*. The first use case, UC 3.1 investigates the battery diagnosis methods and measurement/testing procedures to ensure safety and reliability of battery systems, the second use, UC 3.2 targets the development of affordable high performance testing technologies and methods for 20 kHz e-component testing and assessment methods for battery systems to fulfil performance requirements. The third use case, UC3.3 focuses on the mechanical reliability of the battery system and the last use case, UC 3.4 focuses on control system design from safety perspective.

The following project objective is part of this deliverable:

- Safety and reliability improvement with a factor 10

In the scope of this project, safety is a term strongly related to the functional safety. This means in this context, that it is restricted to the functional and technical properties of the device. Any external safety measures (e.g. a housing covering the entire device) are not considered. Generally speaking, the safety is regarded to consist of 3 major contributors, severity, probability and controllability of the unwanted event. Since the aim is to prevent the failure to happen, controllability was the focus within the project.

The demonstration stages of the use case, the reached improvements are assessed by the involved partners. For each UC, the improvement(s) are calculated in percentage (compared to the SOA/baseline).

2 Introduction

Market penetration of electric vehicles strongly depends on technological and market related factors and also sociocultural and political factors. Political and sociocultural factors are mainly related with incentives, emission regulations, local air quality concerns, rising awareness of consumer and increased urbanization. Market and technological factors are mainly related with charging speed, cost, drive range, infrastructure availability, safety and reliability of the vehicles. The battery is one of the main components of electric vehicles where technological factors are affected and could create a differentiating solution for customers especially on cost, drive range, safety and reliability of the vehicles. When it comes to safety and reliability of the vehicle, batteries play the key role. Testing and development of the battery is a time-consuming process and needs about 2 to 5 years from concept to production phase. Accelerating this development process would therefore quicken the production of the vehicle. Adoption of model-based battery development methods reduces the effort and time and consequently increases efficiency of battery production. Deliverable D6.3 contain the major outputs of use case cluster three as it is shown in Figure 2-1 and focuses on component to vehicle safety and reliability assessment based on simulation and testing methods.

The four considered use cases are UC3.1 '*Battery safety improvement & Testing*', UC3.2 *'20 kHz battery assessment & Testing technologies', UC3.3 'Battery reliability testing and safety improvement*', UC3.4 '*Light commercial demonstrator*'. The first use case, UC 3.1 investigates the battery diagnosis methods and measurement/testing procedures to ensure safety and reliability of battery systems, the second use, UC 3.2 targets the development of affordable high performance testing technologies and methods for 20 kHz e-component testing and assessment methods for battery systems to fulfil performance requirements. The third use case, UC3.3 focuses on the mechanical reliability of the battery system and the last use case, UC 3.4 focuses on control system design from safety perspective.

This use case cluster opens a new pathway to increase the safety and reliability of a battery system by using new measuring approaches which are not implemented yet. A demonstration also shows that the new approaches are applicable in an industrial environment.

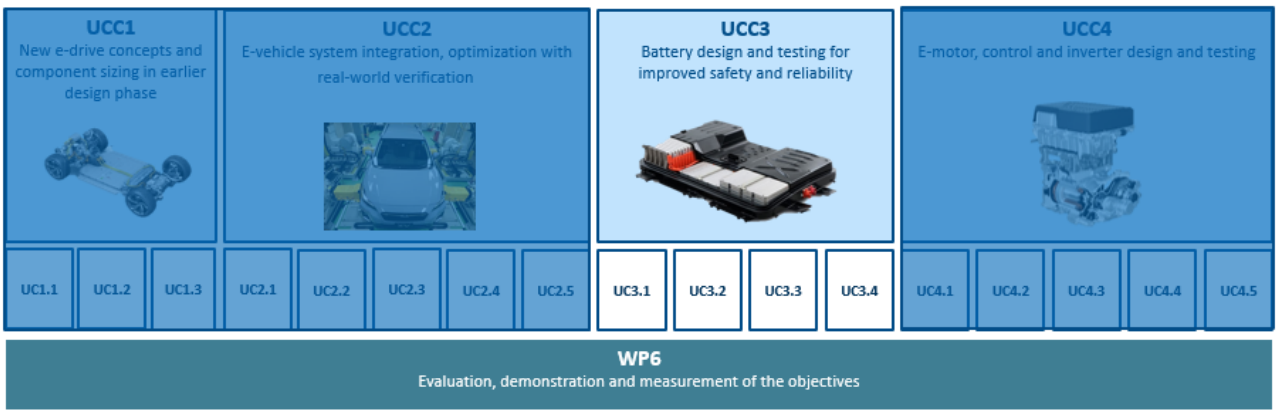

Figure 2-1: Use Case Cluster Structure in Obelics Project

2.1 Purpose and Structure of the document

This deliverable is the 3rd and the last deliverable of WP6. Use case cluster 3 overall results were shared within this deliverable. The deliverable follows the 2 main structure.

This final deliverable D6.3 of WP6 contains the following overviews:

- Publishable executive summary (very brief overview)
- A list of contents
- A list of figures
- A list of tables

Followed by the following main chapters:

- Introduction
- WP6 use case task descriptions & link to other WP results
- Results and Measurement of Task, Evaluation and Conclusion per Use Case
- Project objective evaluation and conclusion
- Risk register
- References
- Acknowledgement
- Appendix

Brief summary of each use case and dependencies over work packages and deliverables were shared under "WP6 use case task descriptions & link to other WP results" section. After that the use case level results, measurements and evaluation section is implemented. Finally, the overall use case cluster level objective evaluation and conclusion section added.

2.2 Deviations from original Description in the Grant Agreement Annex 1 Part A

No deviations were undertaken. The organization of the different subtasks within the deliverable document is described below.

2.2.1 Description of work related to deliverable in GA Annex 1 – Part A

The following table shows, which subtasks from the grant agreement were assigned to this deliverable.

Table 2-1 : Work Related with Deliverable

Task 6.3 Component to vehicle safety and reliability assessment based on simulation and testing methods (Lead: Bosch; Partners: US, FO, AVL, UL, LBF, CEA, Valeo) [M15-36]									
		Bosch	AVL	UL	LBF	CEA	FO	US	Valeo
1	Virtual load data assessment for analyzing reliability and the impact to reduce the generation of load collectives for new vehicles compared to measurements will be investigated and demonstrated. Local vibration profiles on the battery system for different vehicle types will be compared to state-of-the-art testing requirements for battery systems. Finally, lifetime estimation of the demonstrator battery pack will be performed with a focus on vibration loads from state-of-the-art requirements/methods and new generated load collectives to improve the reliability	x	x	x	x	x			
2	Implementation of the embedded electrochemical impedance estimation into the battery pack, with the purpose of measuring the internal temperature of the cells and assessing the reliability of this measurement when performed in conditions representative of a real environment will be executed	x	x		x	x			
3	Verification of the safety-effectiveness of the control algorithm based on ISO 26262 by considering the overall safety of the control systems will be presented, in addition to the focus on specific aspects of the design solution (i.e., architecture, application interfaces and coding) in a virtual environment						x	x	
4	Development of high-performance testing technologies and methods for 20kHz e-component testing including assessment methods for battery systems will be investigated and exposed in a demonstration. Batteries will be tested in the use cases with high frequency components of other EV components	x	x		x	x			x
5	Implementation and testing of the modular, parametric, and fail-safe optimal controller						x	x	
6	Verification of the failsafe and controlled shutdown procedures depending on the final layout of the algorithms developed in WPs 4 & 5 on Xil						x	x	

2.2.2 Time deviations from original planning in GA Annex 1 – Part A

There are no time deviations from the Annex 1 – Part A with respect to the content.

2.2.3 Content deviations from original plan in GA Annex 1 – Part A

There are no deviations from the Annex 1 – Part A with respect to the content.

3 Use Case Description & Link to Other Work Package Results

This section gives an overview about the use cluster 3 use cases and also interaction with work packages within the Obelics project.

The following subtasks have been executed to bring the demonstration of UC3.1, UC3.2, UC3.3 and UC3.4 to a good end and fulfil the project goals:

Component to vehicle safety and reliability assessment based on simulation and testing methods (T6.3.1)

The purpose is to verify in the defined UCs: i) the safety improvement of e-powertrain (on the battery system), ii) the control algorithm by experimenting in a virtual and physical environment according to the standards and considering all the theoretical and technological solutions developed in the project. More use case details are given below:

- Virtual load data assessment for analyzing reliability and the impact to reduce the generation of load collectives for new vehicles compared to measurements will be investigated and demonstrated. Local vibration profiles on the battery system for different vehicle types will be compared to state-of-the-art testing requirements for battery systems. Finally, lifetime estimation of the demonstrator battery pack will be performed with a focus on vibration loads from state-of-the-art requirements/methods and new generated load collectives to improve the reliability (Bosch, AVL, UL, LBF, CEA).
- Implementation of the embedded electrochemical impedance estimation into the battery pack, with the purpose of measuring the internal temperature of the cells and assessing the reliability of this measurement when performed in conditions representative of a real environment will be executed (CEA, Bosch, AVL, LBF).
- Verification of the safety-effectiveness of the control algorithm based on ISO 26262 by considering the overall safety of the control systems will be presented, in addition to the focus on specific aspects of the design solution (i.e., architecture, application interfaces and coding) in a virtual environment (US, FO).
- Development of high-performance testing technologies and methods for 20 kHz e-component testing including assessment methods for battery systems will be investigated and exposed in a demonstration. Batteries will be tested in the use cases with high frequency components of other EV components (AVL, Bosch, Valeo, CEA and LBF).

Safety and reliability assessment on vehicle level (T6.3.2)

The aim is to prove the safety enhancement on a vehicle level for the Ford Otosan UC. The following tasks are foreseen:

1. Implementation and testing of the modular, parametric, and fail-safe optimal controller on the xil (US, FO).
2. Verification of the failsafe and controlled shutdown procedures depending on the final layout of the algorithms developed in WPs 4 & 5 (FO,US).

The following paragraphs demonstrates the results and evaluation of UC3.1, UC3.2, UC3.3 and UC3.4.

3.1 Use Case 3.1 Battery Safety Improvement & Testing Through the Electrochemical Impedance Spectroscopy and The Development of a Cell Model (CEA)

CEA work is focusing on enhanced measurement techniques applied to the battery-cell, based on electrochemical impedance estimation. We can rely upon a solid background of online and offline impedance estimation technique, dedicated procedures for active and wideband or passive cell activation, specific algorithms and a prototyped platform for parameter estimation (temperature) using impedance value as an input on one cell.

The purpose of our contribution to OBELICS is to propose a method that can help the vehicle manufacturer to identify some meaningful parameters of the battery-cells, shortening the building time as the parameter estimation can be done after the battery-pack assembly, in a kind of set-up time of the vehicle before its market introduction.

3.1.1 Technical content and link between Use Case 3.1 and task 6.3

Implementation of the embedded electrochemical impedance estimation into the battery pack, with the purpose of measuring the internal temperature of the cells and assessing the reliability of this measurement when performed in conditions representative of a real environment is executed under T6.3.1.

Technical content	WP6 Sub-task
UC3.1	
Implementation of the embedded electrochemical impedance estimation into the battery pack, with the purpose of measuring the internal temperature of the cells and assessing the reliability of this measurement when performed in conditions representative of a real environment will be executed (CEA, Bosch, AVL, LBF).	6.3.1

3.1.2 Link of Use Case 3.1 to other WP results

Work Package 5 focuses on safety and reliability in electrical vehicles. Contribution of CEA consists in the development of an algorithm dedicated to the diagnostic of thermal state of Li-Ion battery cells, in order to detect temperatures likely to lead to thermal runaway, and based on pure electrical measurement (Electrochemical Impedance Spectroscopy) instead of embedding heat sensors in the battery module. It is closely related to Task 5.2, specifying “impedance estimation into safety concept (CEA)”.

3.2 Use Case 3.2 20 kHz Battery Assessment & Testing Technologies (AVL)

For battery testing, it is necessary to generate test sequences that allow the evaluation of design parameters and formal target specifications as well as the performance under real driving conditions. The test sequences consist of the electrical load profile (charge- and discharge current at the battery terminals) and the environment conditions (air and coolant temperature, initial state of charge, mechanical vibration load).

Regarding the electrical load profile, it is important to assume not only a smooth DC battery current, but to consider the superimposed AC components of the battery current. These are mainly caused by the traction inverter(s) and by other power electronic components connected to the high voltage DC bus. The frequency content ranges from a few Hz caused by power fluctuations due to powertrain oscillations, through several hundred Hz caused by the electric machine's torque ripple and up to tens of kHz related to the switching frequency of the drive inverter.

With the application of wide bandgap power semiconductors to traction drive inverters, the switching frequencies are increased, the DC bus filters can be made smaller. This changes the spectral distribution of the battery current and needs to be considered during the battery test process.

3.2.1 Technical content and link between Use Case 3.2 and task 6.3

Creating realistic load conditions as they would be caused by power electronic converters in the vehicle - including AC current ripple - is necessary to evaluate the safety of a battery pack design already on the testbed with a high degree of fidelity.
As a part of sub-task 6.3.1, the SiC-based electrification test system was applied as a battery pack tester. In order to demonstrate its capability to control not only a DC charge/discharge current, but also high frequency AC components, it was operated back-to-back against a battery pack emulator. The results of this test are reported in this document and the improved testing capabilities are linked to an increase in battery pack safety.

Technical content	WP6 Sub-task
UC3.2	
Development of high performance testing technologies and methods for 20kHz e-component testing including assessment methods for battery systems will be investigated and exposed in a demonstration. Batteries will be tested in the use cases with high frequency components of other EV components (AVL, Bosch, Valeo, CEA and LBF).	6.3.1

3.2.2 Link of Use Case 3.2 to other WP results

For battery testing, it is necessary to generate test sequences that allow the evaluation of design parameters and formal target specifications as well as the performance under real driving conditions. The test sequences consist of the electrical load profile (charge- and discharge current at the battery terminals) and the environment conditions (air and coolant temperature, initial state of charge, mechanical vibration load). Within WP3 it was shown how electric powertrains can be simulated in real-time. Thus, it is possible to generate the battery test profiles on the fly from a vehicle simulation model instead of pre-recording the driving cycles on the road. The results presented in deliverable D3.5 show the real-time simulation of high-speed processes within the power electronic converters such that also high-frequency AC components of the battery current can be derived from simulation models and then be used for battery pack testing. Such profiles can then be applied to battery testing on cell level, module and pack level.

WP4 and in particular D4.2 re-stated the battery testing requirements, when power converters with wide-bandgap power semiconductors will be part of the electric powertrain. The core technologies for building the demonstrated battery test system (SiC-based power converters for application in test systems and fast model predictive control) have been worked out in sub-task 4.2.1 as reported also in D4.2.

3.3 Use Case 3.3 Battery Reliability Testing & Safety improvement (BOSCH)

UC 3.3 is dedicated to the reliability and safety of the battery system in the electric vehicles. The battery itself and the entire system have raised high expectations in electric vehicles. The most important requirement on a battery system is the safety over the entire lifetime of a vehicle. There are two major classifications in terms of lifetime or reliability for a battery system: mechanical and electrical reliability. To describe the system reliability of the battery pack both classifications have to be combined. The mechanical reliability is relevant for structural components, electrical tabs and all kinds of joining's. The electrical reliability needs to be considered for the battery cell and control electronics in the BMS.

Comprehensive technical understanding and appropriate testing facilities are therefore required to deal with the complexity of battery systems with respect to construction, load, functional and damage mechanisms. The most difficult requirement here is the assumption of loads (mechanical and electrical) to ensure a high reliability and safety. These assumptions can strongly depend on the vehicle type and drivetrain configuration. Therefore, it is necessary to have reasonable load data in an early development process to decrease the number of design iterations, which leads to reduced development and testing costs. Consequently, the main goal of this UC is the evaluation and analysis of acting mechanical loads on to the battery system under real driving conditions. The origin of mechanical loads on a battery system can be an internal or external source. Internal loads can be caused by thermal loads from different sources as the swelling behavior of the battery cell or overcharge or any other conditions. External loads are mainly classified in vibration and shock loads. Crash loads will be not covered in the framework of this project. The focus in this project is the description and analysis of external vibration loads on the battery system.

The focus of UC 3.3 was set to the vibrational loading of the battery system. The first aim was to compare the internal loads to existing standards in order to derive conclusions for future test procedures and to evaluate the influence of temperature and state of charge on the vibration response of the battery system. A second aim was to evaluate different approaches to simulate the vibration transfer path from the road to the battery system for monitoring concepts. Monitoring means an approach to calculate the remaining lifetime of mechanical components or to detect critical loading scenarios on the battery. The affected components could be a cell pack housing, fixing ribbons or electrical connectors between cells.

3.3.1 Technical content and link between Use Case 3.3 and task 6.3

The vibration response of a vehicle battery was extensively studied in a wide range of parameters. The goal was to detect critical operational states which should be implemented in the validation testing of the battery. The virtual load data assessment can be used as generator for load collectives of different rough road tracks.

Technical content	WP6 Sub-task
UC3.3	
Virtual load data assessment for analysing reliability and the impact to reduce the generation of load collectives for new vehicles compared to measurements will be investigated and demonstrated. Local vibration profiles on the battery system for different vehicle types will be compared to state of the art testing requirements for battery systems. Finally, lifetime estimation of the demonstrator battery pack will be performed with a focus on vibration loads from state of the art requirements/methods and new generated load collectives to improve the reliability (Bosch, AVL, UL, LBF, CEA).	6.3.1

3.3.2 Link of Use Case 3.3 to other WP results

UC3.3 was mainly linked to WP 4 and WP 5. The vibration measurement campaign on the vehicle and as well on the test bench were part of WP 4. The modeling of the vibration transfer behavior was done in WP5.

3.4 Use Case 3.4 Battery Reliability Testing & Safety Improvement (US&FO)

UC3.4 is aimed to advance the current software (SW) development process, along with enhancement of the overall safety and reliability of the safety-critical embedded SW in electric vehicles. The technological progress in the field of high-voltage-batteries, electrical machines and race for optimisation of powertrain efficiency has led an evolution in the automotive industry, resulting in vehicle manufacturers to shift towards electrified powertrains. Hence, the number of ECUs, which accommodates embedded SW, has increased. This resulted in increase of not just the size but also complexity and SW sophistication. As a result, the safety of the embedded SW has become a key challenge for the automotive, and Tier 1 supplier.

The focus of the Use Case 3.4 is on the improvement of the safety of the electrified powertrain through the use of systematic, analytic, objective development process and safe by design (SbD) approach for the safety critical embedded SW. To enhance the safety of the SW both the development process and the safe code development phase are considered in the scope of the UC3.4. Accordingly, firstly the US come up with a systematic, analytical and objective SW development approach to ensure that electrified road vehicle algorithm developments conform to ISO26262. Secondly, the US and Ford Otosan developed together flexible and safe start-up and shutdown sequence controller enabling vehicle to reach safe state when encountering random temperature faults and communication errors during the daily operation routine of the vehicle. Thirdly, a modular safety integrated energy management algorithm is developed that moderates the torque to mitigate unsafe consequences of the failure during the vehicle operation. Lastly, a modular fault tolerant algorithm is developed that allocates the torque between EMs of an all-wheel drive electric refuse truck in case of an abrupt additive temperature fault based on the risk decision unit. As a result, by proposed systematic, analytical and objective SW development procedure and SbD approach not only the development time is reduced but also failures are identified and mitigated in the early design phase that enhances the reliability and the safety of the SW.

3.4.1 Technical content and link between Use Case 3.4 and task 6.3

Technical content	WP6 Sub-task
UC3.4	
Verification of the safety-effectiveness of the control algorithm based on ISO 26262 by considering the overall safety of the control systems will be presented, in addition to the focus on specific aspects of the design solution (i.e., architecture, application interfaces and coding) in a virtual environment (US, FO).	6.3.1
Implementation and testing of the modular, parametric, and fail-safe optimal controller on the Ford Otosan light commercial demonstrator vehicle with evaluation on the road (US, FO).	6.3.2
Verification of the failsafe and controlled shutdown procedures depending on the final layout of the algorithms developed in WPs 4 & 5 on the Ford Otosan light commercial demonstrator vehicle (US, FO).	6.3.2

3.4.2 Link of Use Case 3.4 to other WP results

UC 3.4 depends on the models presented in the D3.5, and further improved to enable the integration of the safe start-up and shutdown sequence controller together with fault tolerant algorithm according to the targets of the WP5. Results obtained using these methods and approach are presented in the D5.6, D5.7 and D 6.2.

4 Results and Measurement of Task, Evaluation and Conclusion per Use Case

4.1 Use Case 3.1

No changes of the use-case/evaluation methodology.

4.1.1 Demonstration

No changes from what is presented in WP4 and WP5 deliverables.

4.1.2 Results and Measurements

4.1.2.1 Experimental work and first analysis

Electrochemical Impedance Spectroscopy (EIS) measurements were performed by the means of appropriate laboratory equipment on two Li-ion cells "LG_HG2", for temperatures going from 10 °C to 60 °C by steps of 10 °C, and for different States of Charge (SoC): 10 %, 25 %, 50 %, 75 %, 100 %. By instance, the Nyquist diagrams for all mentioned temperatures at SoC=100 % are depicted here below in Figure 4-1. The frequency range is between 0.1Hz (the upper-right point) and 10 kHz (the lower-left point).

The two cells exhibit an extremely similar behavior, with a small impedance difference in the "inductive branch" (corresponding to high frequencies, lower-left point mostly). Measurements performed on only two cells being not sufficient to conduct a "dispersion study", we chose to focus on one of those two only; nevertheless, for further developments, it must be considered that several models parameters exposed below (in particular : resistances R1 and R2, and inductance L) are statistically distributed for a sample of the same product.

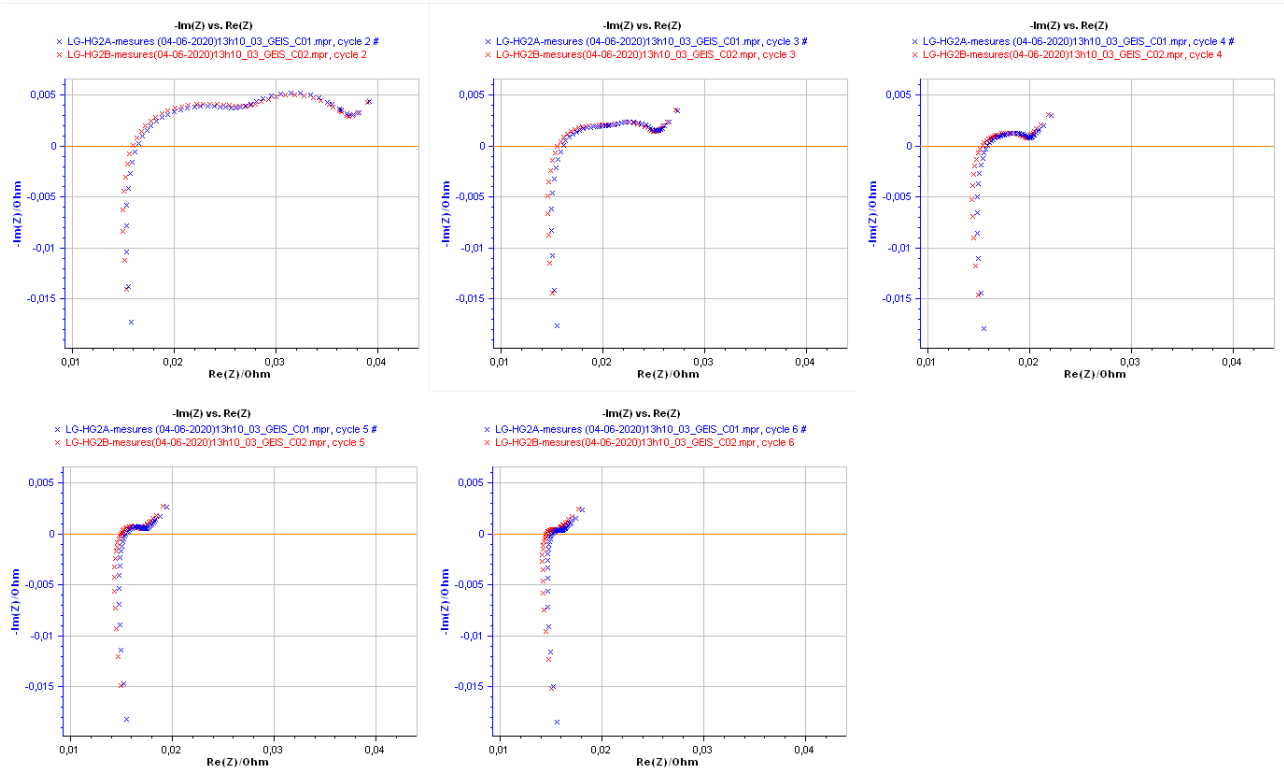

Figure 4-1: Nyquist diagram of a LG cell at SoC=100% and at every tested temperature.

We clearly notice that the "width" of the Nyquist plot notably reduces with the temperature, which makes the temperature estimation of the cell from the EIS measurement, a promising solution. We can distinguish three main regions in those plots:

1. At low frequency, we observe an almost-constant slope, called the diffusion branch. It corresponds to the diffusion of Li-Ion atoms in the electrode particles.
2. At medium frequency, we observe one or two ellipses, corresponding to the diffusion of Li-Ion in the electrode thickness.
3. At high frequency, we observe an inductive behavior.

It is important to notice that the boundaries between those different domains depend on the temperature. The "inflexion point" at the left of the diffusion branch corresponds to a frequency of 0,4 Hz at 10 °C, and 10 Hz at 50 °C. In the same way, the crossing point with the real axis in the inductive branch corresponding to a purely resistive impedance (Im(Z)=0, the imaginary part of the impedance is zero) is 1200 Hz at 10 °C and 300 Hz at 50 °C. Those dependencies may be used to estimate the temperature (but the second solution, often called zero-crossing approach in literature, is more practical and embeddable, as high-frequency measurements are faster to perform).

Finally, as clearly seen in those plots, the "width of the middle region" is strongly dependent on the temperature and can be used as well to estimate the temperature. In the parameters set of the model presented above, it is correlated to the quantity R2+R3.

4.1.2.2 EIS model

We now expose the proper model used to reproduce this behavior. The "twisted-capacitor" symbols are **Constant Phase Elements** (CPE). They correspond in the Nyquist plane to lines with constant slopes (a classical standard component, as a capacitor, would not give such a plot). Put in parallel with a resistor, it leads to sorts of pieces of ellipses, appropriate to represent the harmonic behavior of electrodes. Resistance R1 is used to shift the entire Nyquist diagram to the right (growing resistance), and inductance L is useful to adjust the high frequency behavior. We have chosen not to model the diffusion branch, which corresponds to low frequency, because it leads to measurements taking more than 0.1 seconds to be performed, onerous during normal use in embedded systems. Thus, the CPE represented by parameters Q4 and a4 is subsequently removed from the model.

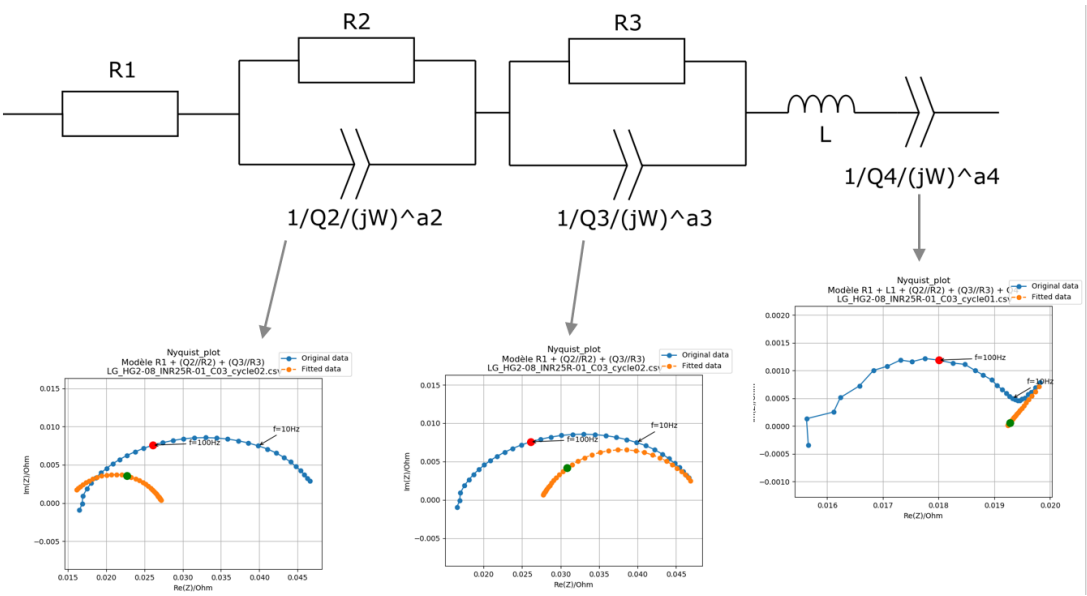

Figure 4-2: Graphical representation of the Li-ion cell model, highlighting the contributions of each part

4.1.2.3 Set of parameters evaluated to reproduce the measurements

The entire parameters table obtained by the means of optimized identification process, at each temperature and SoC, is represented here below:

SoC 100%	10°C	20°C	30°C	40°C	50°C
R1 (Ohm)	0,01418	0,01351	0,01319	0,01298	0,01287
Q2 (F)	8,939	8,939	8,939	8,939	8,939
a2	0,851	0,851	0,851	0,851	0,851
R2 (Ohm)	0,01092	4,90E-03	2,55E-03	1,38E-03	8,17E-04
Q3 (F)	0,9494	0,9494	0,9494	0,9494	0,9494
a3	0,627	0,627	0,627	0,627	0,627
R3 (Ohm)	0,01361	7,48E-03	4,68E-03	3,29E-03	2,56E-03
L (H)	2,86E-07	3,10E-07	3,34E-07	3,56E-07	3,57E-07

Figure 4-3: Model parameters values at SoC = 100%.

SoC 75%	10°C	20°C	30°C	40°C	50°C
R1 (Ohm)	0,01425	0,01369	0,01352	0,01353	0,01407
Q2 (F)	9,249	9,249	9,249	9,249	9,249
a2	0,82	0,82	0,82	0,82	0,82
R2 (Ohm)	2,13E-03	1,15E-03	6,30E-04	4,07E-04	5,43E-04
Q3 (F)	0,8874	0,8874	0,8874	0,8874	0,8874
a3	0,638	0,638	0,638	0,638	0,638
R3 (Ohm)	1,27E-02	6,98E-03	4,18E-03	2,60E-03	1,12E-03
L (H)	2,99E-07	3,20E-07	3,18E-07	3,17E-07	3,03E-07

Figure 4-4: Model parameters values at SoC = 75%.

SoC 50%	10°C	20°C	30°C	40°C	50°C
R1 (Ohm)	0,01445	0,01388	0,01377	0,01376	0,01409
Q2 (F)	9,249	9,249	9,249	9,249	9,249
a2	0,82	0,82	0,82	0,82	0,82
R2 (Ohm)	1,73E-03	9,94E-04	6,17E-04	4,21E-04	4,29E-04
Q3 (F)	0,8874	0,8874	0,8874	0,8874	0,8874
a3	0,638	0,638	0,638	0,638	0,638
R3 (Ohm)	1,32E-02	7,21E-03	4,23E-03	2,52E-03	1,34E-03
L (H)	2,98E-07	3,15E-07	3,16E-07	3,15E-07	3,08E-07

Figure 4-5: Model parameters values at SoC = 50%.

SoC 25%	10°C	20°C	30°C	40°C	50°C
R1 (Ohm)	0,01397	0,0137	0,01363	0,01367	0,01398
Q2 (F)	9,249	9,249	9,249	9,249	9,249
a2	0,82	0,82	0,82	0,82	0,82
R2 (Ohm)	1,85E-03	1,12E-03	6,60E-04	4,76E-04	4,16E-04
Q3 (F)	0,8874	0,8874	0,8874	0,8874	0,8874
a3	0,6377	0,6377	0,6377	0,6377	0,6377
R3 (Ohm)	8,15E-03	4,79E-03	2,99E-03	1,88E-03	1,07E-03
L (H)	2,53E-07	2,63E-07	2,64E-07	2,63E-07	2,58E-07

Figure 4-6: Model parameters values at SoC = 25%.

SoC 10%	10°C	20°C	30°C	40°C	50°C
R1 (Ohm)	0,01557	0,01468	0,0143	0,01393	0,01386
Q2 (F)	9,249	9,249	9,249	9,249	9,249
a2	0,82	0,82	0,82	0,82	0,82
R2 (Ohm)	4,16E-02	1,51E-02	6,98E-03	3,40E-03	1,99E-03
Q3 (F)	0,887	0,887	0,887	0,887	0,887
a3	0,64	0,64	0,64	0,64	0,64
R3 (Ohm)	1,83E-02	9,81E-03	5,77E-03	3,91E-03	2,73E-03
L (H)	2,33E-07	2,33E-04	2,33E-07	2,76E-07	2,76E-07

Figure 4-7: Model parameters values at SoC = 10%.

To obtain those tables, we have fixed values of Q2, a2, Q3 and a3 (or let them vary very slightly), and determined the remaining parameters in order to obtain the bests fits with data. Example of the approach:

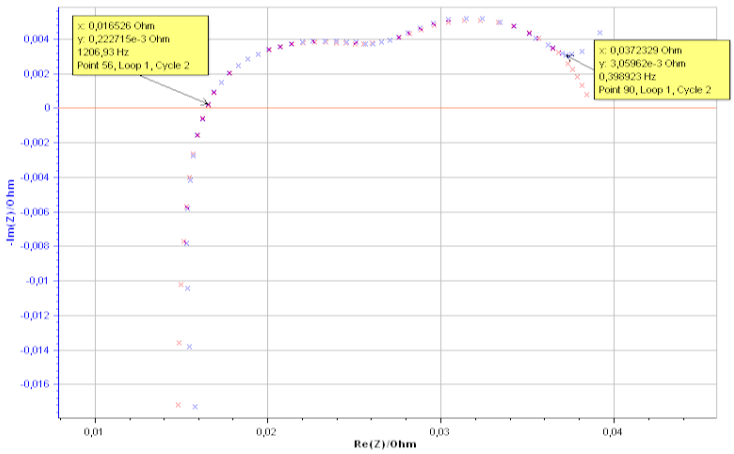

Figure 4-8: Example of the approach used to determine the model parameters.

We can now focus on the evolution of those parameters 'Resistance' as a function of temperature and SoC:

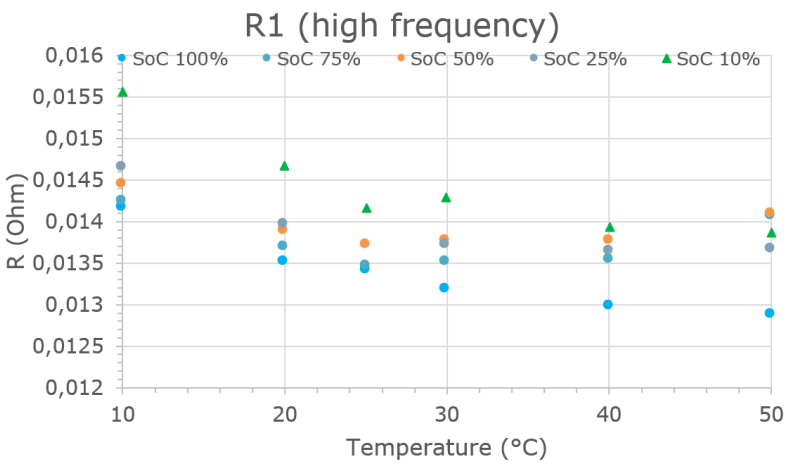

Figure 4-9: Dependency of the R1 parameter as a function of temperature and SoC.

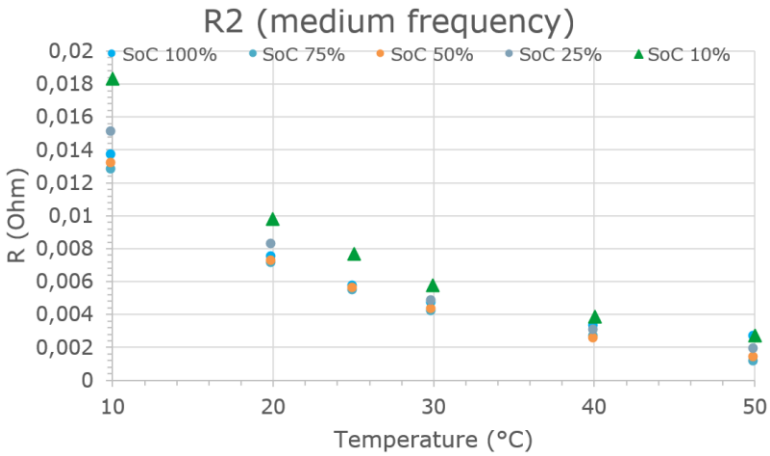

Figure 4-10: Dependency of the R2 parameter as a function of temperature and SoC.

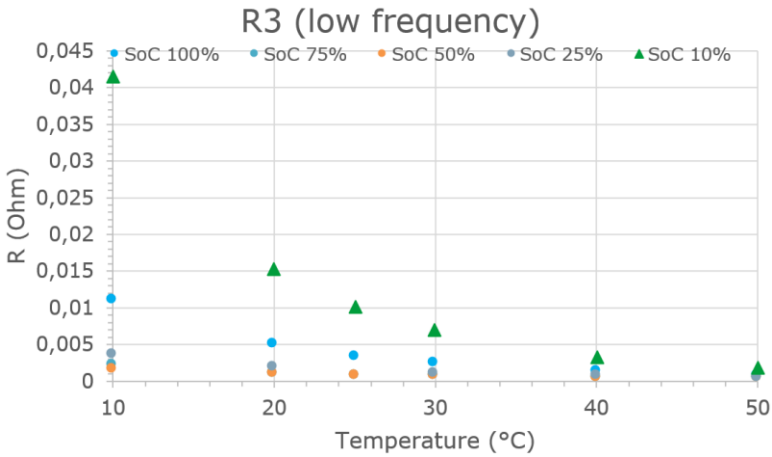

Figure 4-11: Dependency of the R3 parameter as a function of temperature and SoC.

We observe that R1 is mostly independent from the temperature, whereas R2 and R3 plots reveal clear dependencies.

4.1.2.4 Building temperature estimator

The two resistances R2 and R3 can be very hard to distinguish in the Nyquist plot at high temperature; it appears wiser to examine the quantity R2+R3 (which is strongly correlated to the ”width” of the Nyquist plot) :

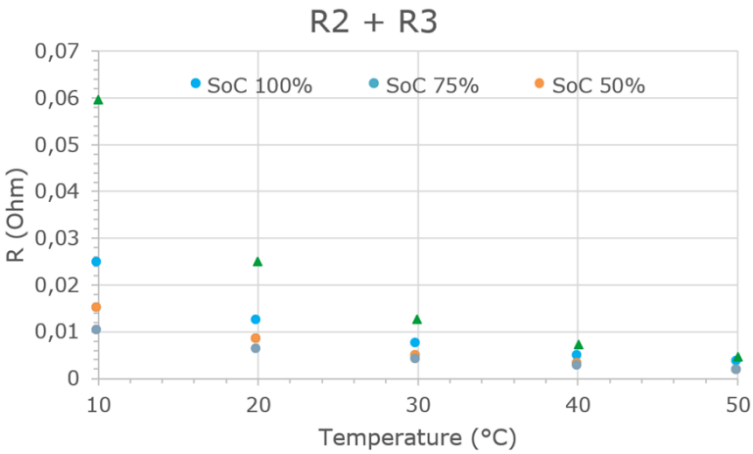

Figure 4-12: Dependency of the “R2 + R3 parameter as a function of temperature.

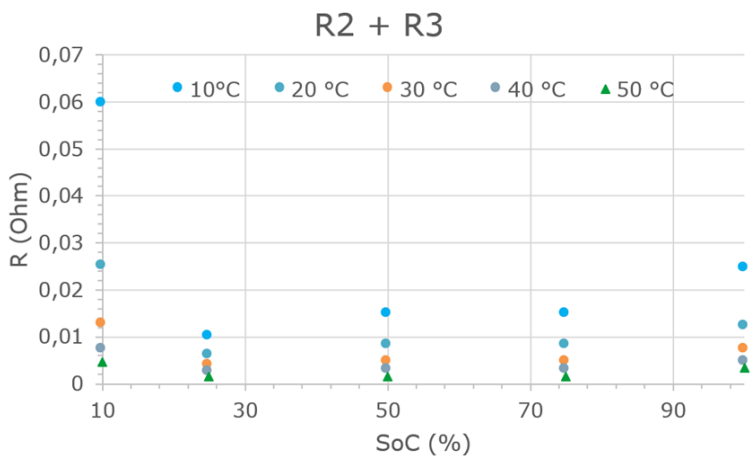

Figure 4-13: Dependency of the "R2 + R3 parameter as a function of SoC.

The function (R2+R3)(T) being monotonous and quite smooth for a given SoC, we expect that it is possible to build an embedded temperature estimator on the basis of this quantity R2+R3 in the studied range if the SoC is known.

The other considered way is building an estimator by looking at the frequency at which the Nyquist plot crosses the real axes (Im(Z)=0). The plots of this quantity are the following:

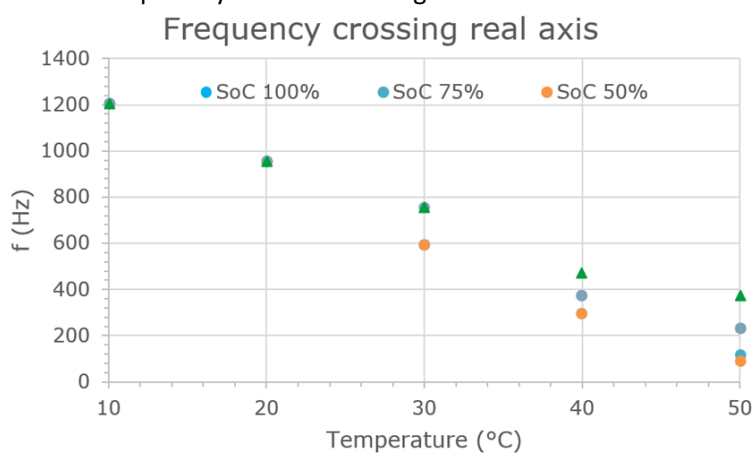

Figure 4-14: Imaginary part of the impedance 'zero-crossing' frequency as a function of temperature.

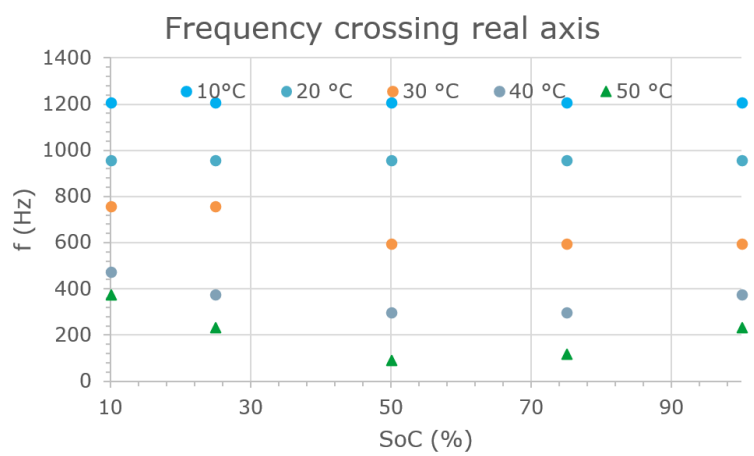

Figure 4-15: Imaginary part of the impedance 'zero-crossing' frequency as a function of SoC.

4.1.3 Evaluation

The dependency of this frequency on SoC is very slight at low temperature, but becomes significant at higher temperature. Note that due to a weak sampling in this region - as we did not initially plan to focus on this point – the specified values of frequency are subject to imprecision, which however may not compromise the observed tendency.

The dependency of this frequency on temperature is very clear and can be exploited to build a cell temperature estimator by the exploitation of indirect measurements.

4.1.4 Conclusion

The general purpose of our work in the framework of the UC3.1 was to address and explore the possibility to determinate the state of a Lithium-ion battery cell by using indirect measurements. This goes with the general idea of Smart Cell: a battery cell equipped with an embedded electronic system and optionally with some sensors, which give it smart features, as communication capabilities or self-measurement. More precisely, we adapted the well-known Electrochemical Impedance Spectroscopy into an embedded system - an electronic device based on an STM32 microcontroller – performing the impedance estimation by cell activation and voltage-current acquisition, the whole followed by onboard computation. This device was directly connected to a Li-ion cell and tested at different temperature levels. The results we had were a certain number of so-called “Nyquist diagrams”, depicting the variations of the impedance of the cell. However, this is only the preliminary part of the work. The following step of our approach was based on the development of a cell model, based on virtual discrete components, calibrated on real tests that were performed on a Li-ion cell and, this time, by using standard electrochemical Impedance Spectroscopy Laboratory equipment. Some reference Nyquist diagrams were obtained this way for each cell condition, in terms of cell temperature and State of Charge, allowing us to determine some useful and observables parameters that may be furtherly exploited to retrieve the cell state during normal use. The final step is the exploitation of the results obtained in the two described ways, by comparing them. We started from the assumption that, with the quite satisfactory accuracy of the embedded electronics results, we can determine some “points” or observable parameters of the Nyquist diagram, that have a direct correspondence between what is obtained from the embedded tests and what is predicted by the theoretical model. Tracing the evolution of these points, calculating the difference between the tested and the predicted ones – the “residuals” and then classifying them, the state of the cell can be predicted. In practical terms, as long as the difference stays below some pre-determined thresholds, the cell can be assessed as safe; if a drift of some or all of these meaningful points is detected, that means that the cell is exiting its normal and predictable state, possibly entering in a dangerous zone of function like the apparition of a thermal runaway, eventually exploding or burning. The major advantage of this technique would be, in the future, the improvement of the safety of the battery, without complexing too much its hardware architecture. One example for all: the cell temperature can be retrieved without any thermal sensor deployed in the proximity or even inside the cell.

From the safety improvement point of view, the achievement of this approach can be reformulated as follows.
According to the literature, the probability of occurrence of an internal short-circuit capable of provoking the thermal-runaway for a 18650 cell is of 0,1 ppm (or 10E-7) *[13].* During normal use inside a battery pack, this probability rises to 10E-5 in the worst case. This assumption takes into account the external or internal events (shocks, over temperature, short-circuits, acid attacks...) or even some manufacturing problems that can provoke the thermal runaway of a cell, as well as other critical events (like gas emission). From now on, we simply focus on the “thermal runaway”, defined as an unstoppable and exothermal reaction of the components of a cell. We estimate that 95% of dangerous states bringing to thermal runaway can be detected by our system, leaving only 5% of 'false negative'. The improvement factor is so estimated to be 95% of detection of all technically possible thermal runaway situations.

4.2 Use Case 3.2

Difference to methodology outlined in D1.4: For the demonstration, no real battery pack was available to be used as test specimen for the battery pack tester. As a substitute, the battery pack was emulated using a battery emulator with equivalent circuit parameters derived from real cells.

4.2.1 Demonstration

A prototype of the SiC-based battery pack tester was used to test the ability of injecting an AC current into the test specimen at the battery pack level. The following Figure 4-16 shows a photograph of the test setup. The battery pack tester can be seen on the right-hand side. The battery pack was emulated using the same type of test system acting as a voltage source, which tracks the voltage response of a virtual battery pack subjected to the measured charge/discharge current.

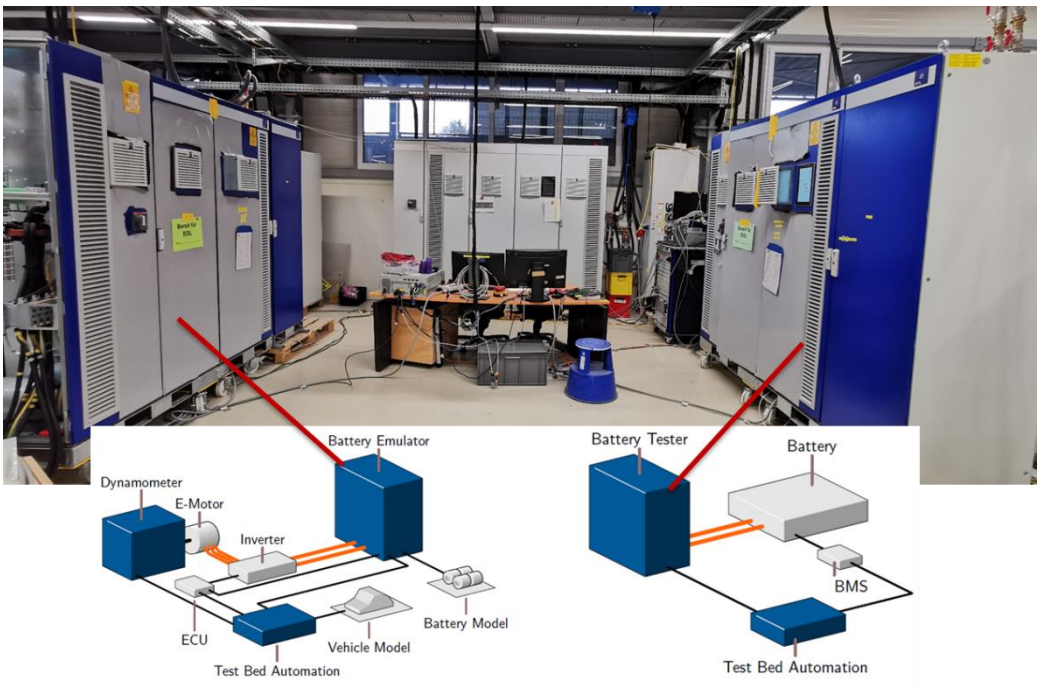

Figure 4-16: Back-to-Back test setup for evaluation of the SiC-Based battery pack tester.

The following figures show the result of the back-to-back tests. Figure 4-17 shows a comparison between real and emulated battery pack subjected to a DC discharge current. The battery model parameters were derived from a measurement with single cells as they are part of the battery pack of a Tesla Model 3. The battery emulation was then implemented with a real-time equivalent circuit model embedded into the model predictive controller of the battery emulator. Figure 4-18, Figure 4-19 and Figure 4-20 show the results of applying an AC current ripple at various frequencies in addition to the DC discharge current.

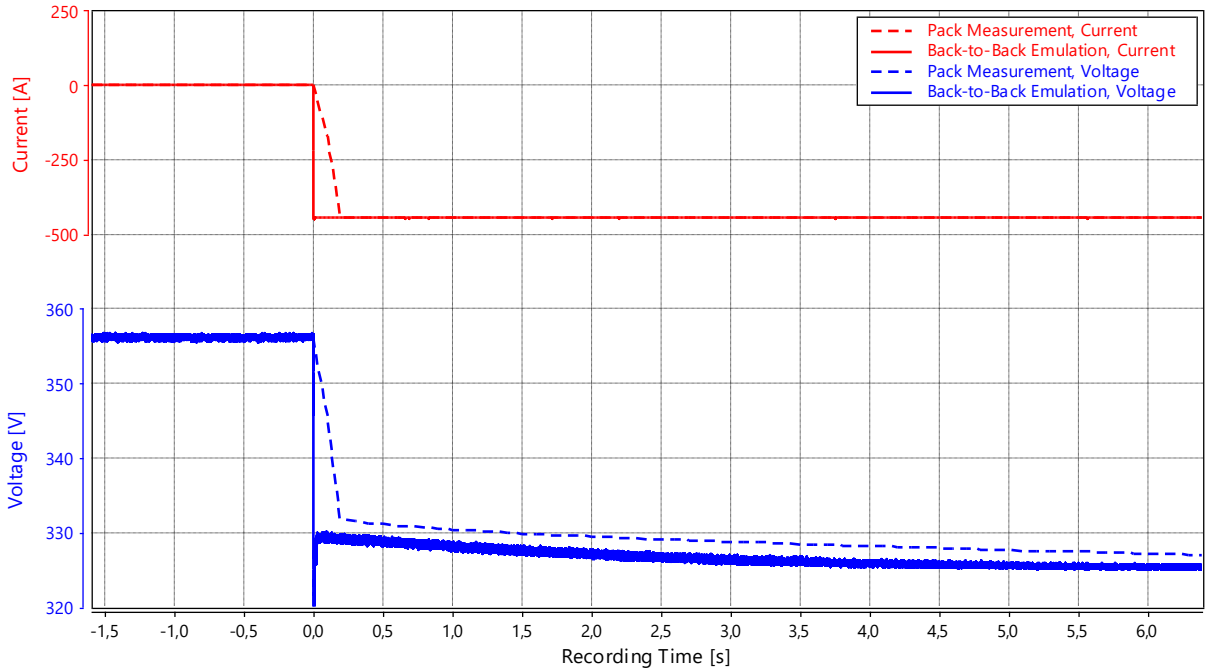

Figure 4-17: Result of Back-to-Back testing with emulation of a battery pack. Comparison between data obtained from a real battery pack on a battery tested and the response of the emulated battery pack subjected to the same load current profile.

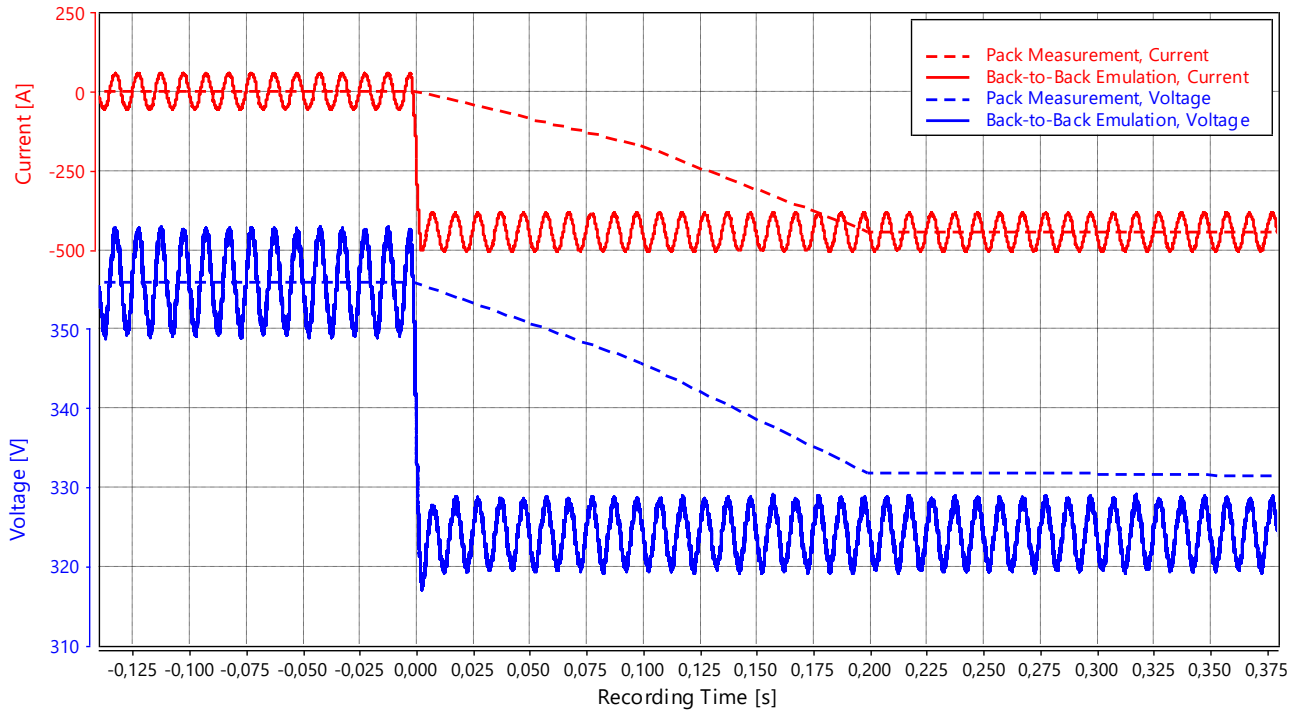

Figure 4-18: Repeated test profile but with a superimposed AC current ripple with a frequency of 100 Hz and an amplitude of 60 A peak.

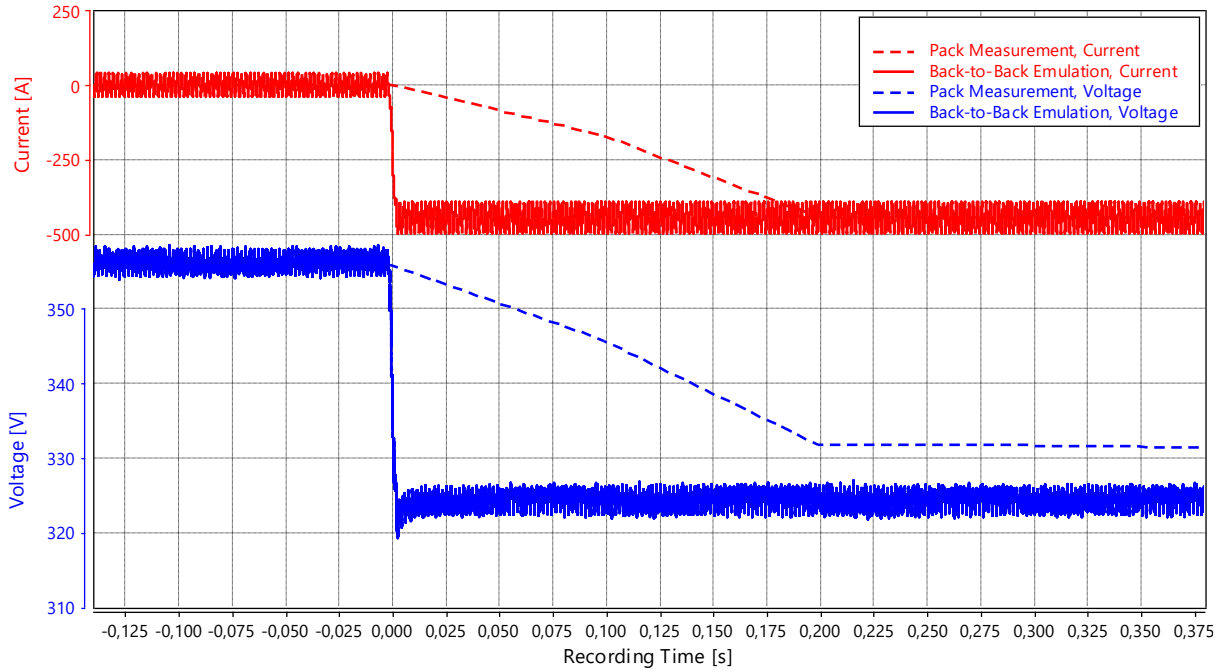

Figure 4-19: Repeated test profile but with a superimposed AC current ripple with a frequency of 500 Hz and an amplitude of 40 A peak.

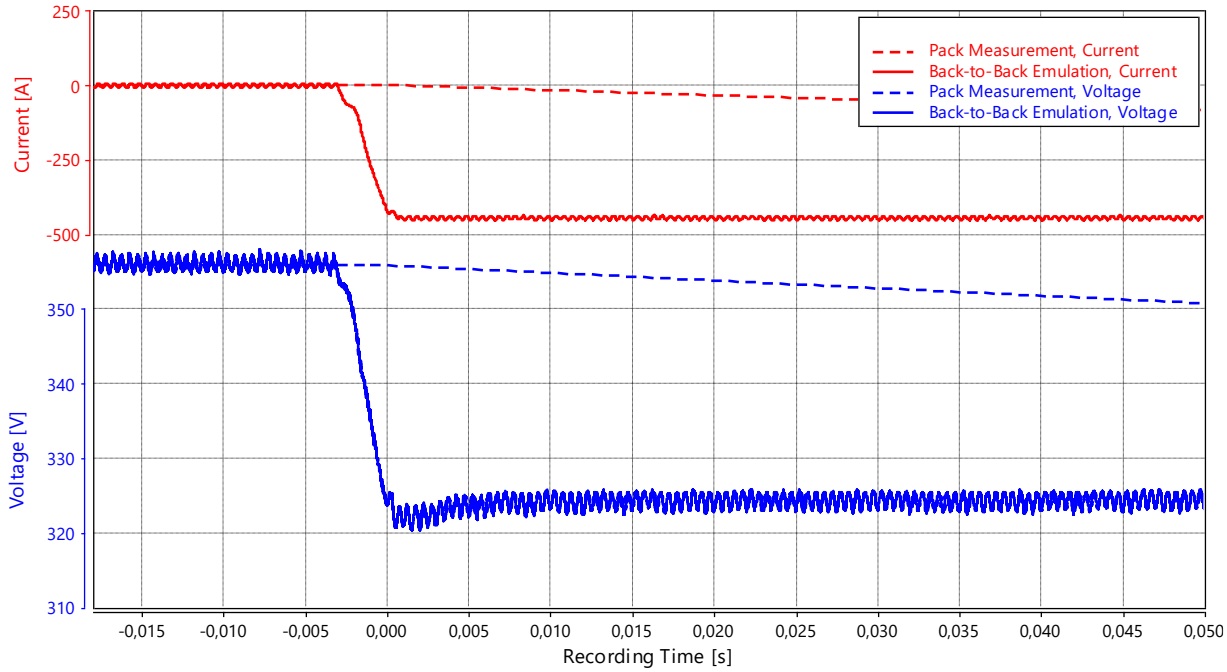

Figure 4-20: Repeated test profile but with a superimposed AC current ripple with a frequency of 2000 Hz. The battery pack tester is still capable of generating this frequency but only with a reduced amplitude of 6 A peak.

The demonstration was carried out with the use of a DSP-based control board, which is not capable of fully utilizing the increased dynamic performance of the SiC power converter. With an FPGA based control board, it would be possible to further increase the closed loop bandwidth with still the same power converter.

Simulations were carried out to demonstrate the increase of bandwidth when using faster control algorithms that can be only implemented on FPGA-based control platforms. The simulation model of the controller is shown in Figure 4-21 and the simulation results in Figure 4-22. The bandwidth can be increased from about 2 kHz to 5 kHz.

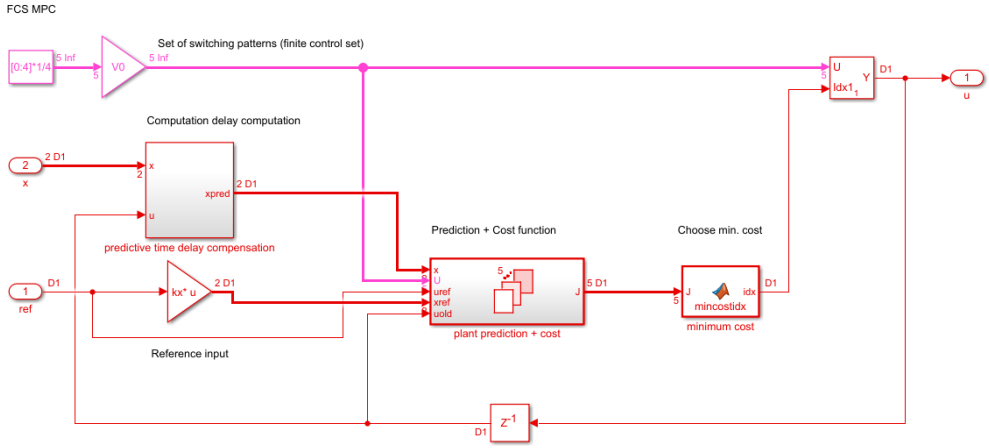

Figure 4-21: Simulation model of a Finite Control Set MPC (FCS-MPC) for interleaved DC/DC converters. Suitable for automation code generation for FPGA target devices.

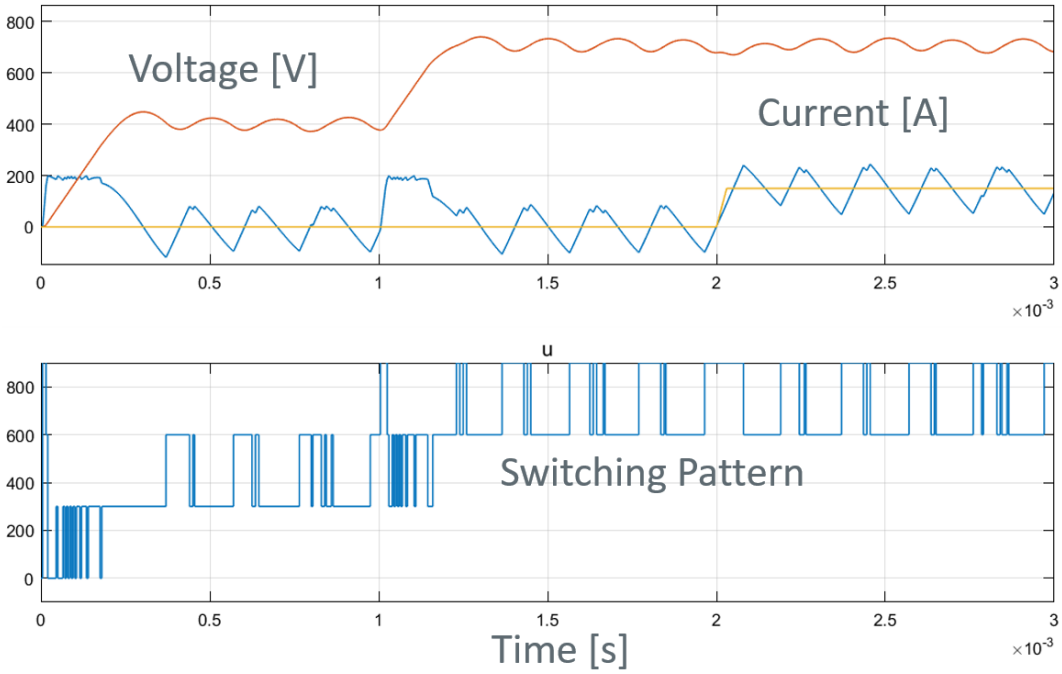

Figure 4-22: Simulation results of FCS-MPC controlled battery pack tester. With the same power converter but an improved controller, it is possible to superimpose an AC current ripple at frequencies up to 5 kHz.

In general, the bandwidth of a high-power DC-source used as battery tester will always be limited. However, the injection of an AC current ripple with even higher frequencies is possible with the use of an external ripple generator.

Such a setup is displayed in Figure 4-23. The resulting superposition of a DC charging current and an AC current ripple at 20 kHz is shown in Figure 4-24.

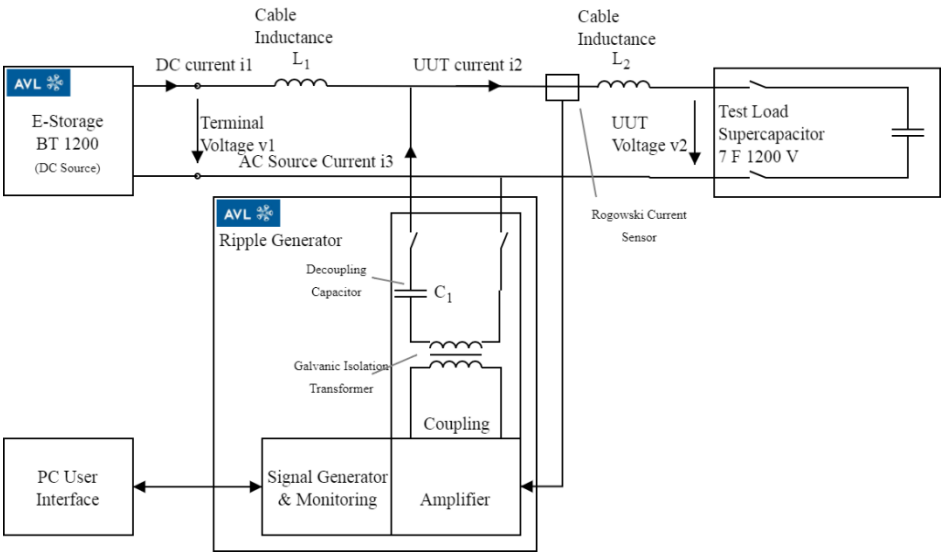

Figure 4-23: High frequency battery testing setup with an external ripple generator.

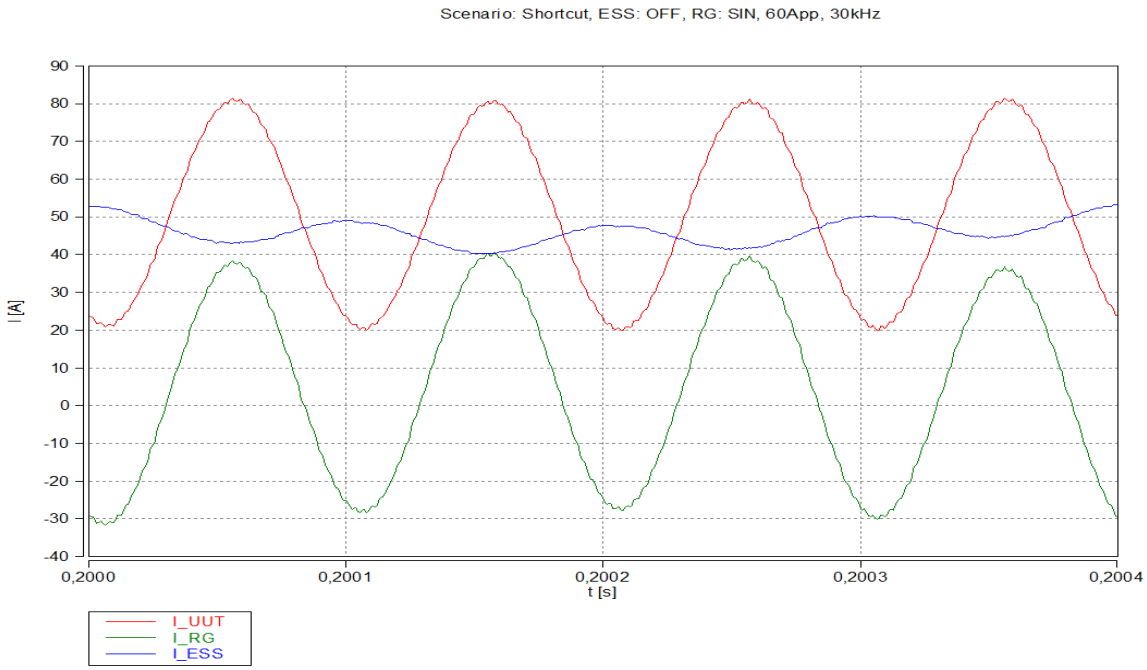

Figure 4-24: Current waveforms recorded with a high frequency battery test setup. Red: battery pack current. Green: external ripple generator output. Blue: output current of battery pack tester.

4.2.2 Results and Measurements

4.2.2.1 Impact on operational safety of the battery pack

The AC component of the battery current has an impact on the degradation of Li-Ion battery cells and hence also on the usable lifetime of traction battery packs. The involved physical effects are various. At lower frequencies up to some tens of Hz it is clear, that the AC current component interacts with the electro-chemical processes inside the cell. At medium frequencies, the intrinsic capacitance of the thin-layered battery cell construction acts as a buffer and it can be expected that electro-chemistry is not affected much. At higher frequencies in the kHz-range, the parasitic inductances of the high-current bus-bars connecting the cells, the capacitances between cells and pack housing and the influence of eddy current effects (skin-effect, proximity effect) determine the frequency response of the battery pack.

Some published studies (for example [9] and [10]) indicate, that also medium and high frequencies influence the cell degradation. But which frequencies have the most deteriorating effect on state of health, and which even have a positive effect, is not fully clear. As a rough indication, [9] and [10] indicate, that low frequencies influence the electrochemistry and thus on the ageing of the cells. Higher frequency ripple (roughly > 1 kHz) has an indirect effect as it increases the self-heating of the cells. Hence, it is important to evaluate and test the influence of AC ripple for each specific battery pack design.

The impact on the battery pack safety is two-fold:

1. The increased cell degradation caused by AC current ripple can lead to early failure of single cells.
2. The increased amount of AC current ripple leads to additional self-heating of the cells and the bus bars and connections between the cells inside the battery pack. The additional heat dissipation may lead to unexpected rise of the temperature in the pack or in the batteries themselves, which can finally lead to a thermal runaway.

The specific AC current ripple spectrum strongly depends on the layout of the vehicle's DC-bus and on the inverter design, including the choice of the DC-filter capacitor and modulation strategies [11], [12]. Hence, this must be evaluated for each specific design.
The heat dissipated inside the battery pack can be calculated with $P_{loss} = I^2R_i$. If the current is not constant but comprises of DC current I_{DC} and AC current I_{AC} (given in A RMS), the $P_{loss} = I_{DC}^2R_{DCi} + I_{AC}^2R_{ACi}$.

As an exemplary case, the Tesla Model 3 battery pack was taken. At 25 °C, the total internal resistance of the pack amounts measured to be approximately 68 mΩ. The largest part is attributed to conduction resistance of cell interconnections and busbars, whereas only a small part is caused by the electrochemical diffusion resistance (approximately 10 mΩ). Hence, R_{DCi} = 68 mΩ and R_{ACi} = 68 mΩ – 10 mΩ = 58 mΩ.

At higher frequencies, the skin effect starts to play a bigger role. The skin depth inside a copper conductor can be approximated with $\delta = 2\mu m\sqrt{1/f[GHz]}$.

For a hypothetical conductor with a cross section of 95 mm² (which is reasonable for the max currents of the considered battery pack), this means, that the effective cross section at 20 kHz is reduced to 14.8 mm². This means further, that the effective resistance of the conductor is 6.4 times higher at 20 kHz than at DC. Hence, for the considered battery pack, the R_{ACi} (20 kHz) = 6.4 x 58 mΩ = 371 mΩ.
If the AC current ripple amplitude amounts to 20% of the DC current, then the dissipated power will become $P_{loss} = I_{DC}^2R_{DCi} + I_{AC}^2R_{ACi} = I_{DC}^2R_{DCi} + (0.2I_{DC})^2\ 6{,}4\ R_{ACi} = I_{DC}^2R_{DCi} + 0.256\ I_{DC}^2\ R_{ACi}$. This corresponds to a 25% increase of the dissipated heat, which is an additional burden for the battery cooling system, and this may lead to local hot spots during short-time peak loads.

The effect on the total dissipated heat during a driving cycle is illustrated in Figure 4-25.

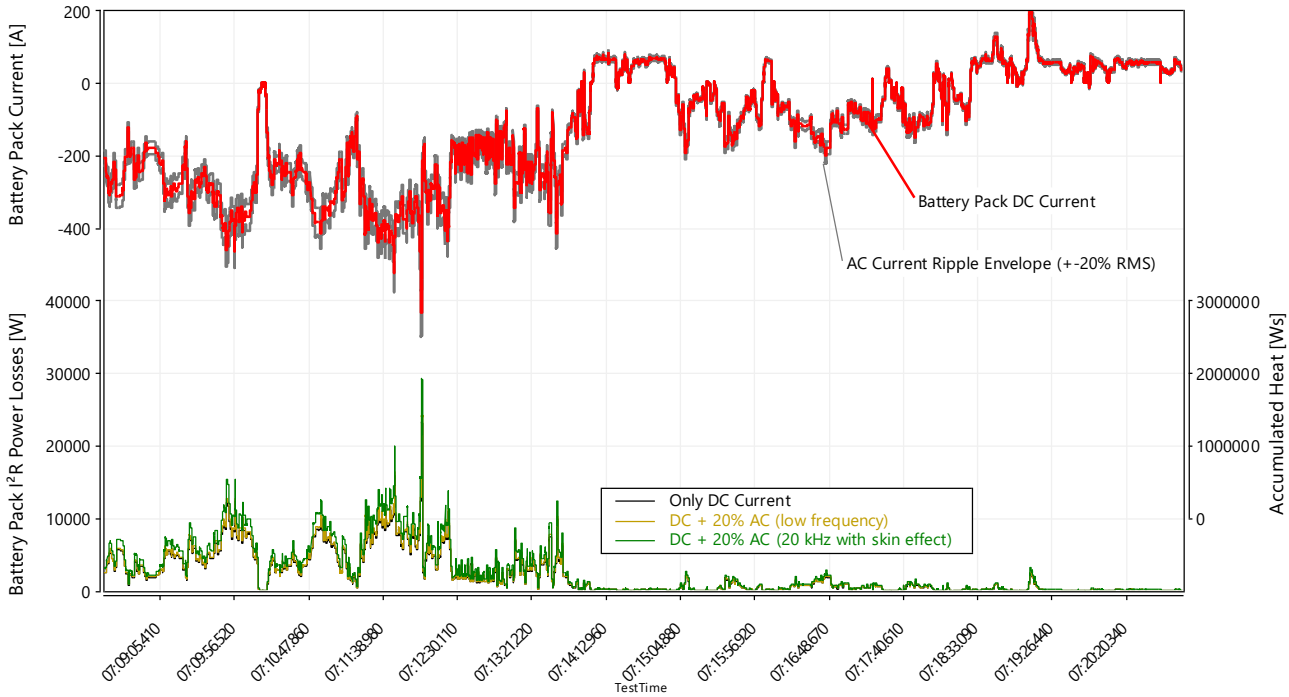

Figure 4-25: Estimation of battery pack heat dissipation due to high frequency ripple current. **Calculations based on data obtained from single cell testing with cells out of a Tesla Model 3 battery pack. The cells were subjected to load current that was recorded during the Graz-Gleisdorf RDE driving cycle. The results were scaled back to the pack level.**

4.2.3 Evaluation

The effect on battery pack safety due to more realistic testing during the development and validation phase is summarized as follows:

More realistic battery pack power losses during tests	Battery pack power loss with only DC testing
37.5 kW	30 kW
$Improvement_{reported}$ = [37.5 kW/30 kW]*100% = 25%	

$X_{measured}$ is based on:	$X_{reference}$ is based on:
Assumed increase of losses due to skin effect in a copper conductor of 95 mm² caused by a ripple current at 20 kHz with AC magnitude of 20% (RMS) of DC current: +25% Example taken: Tesla Model 3 Battery Pack increased losses 30 kW to 37.5 kW with more realistic test conditions -> 7.5 kW extra peak heat load for cooling system. -> Increased risk of thermal runaway	Conduction losses inside battery pack at maximum discharge current (only DC current was tested, no AC current superimposed). Tesla Model 3 Battery Pack peak Thermal losses: 30 kW (corresponds to max. discharge power of 210 kW during Graz-Gleisdorf driving cycle with a measured internal resistance of appr. 58 mOhm)

4.2.4 Conclusion

Towards Use Case 3.2, the project OBELICS resulted in a set of tools that can be used for more realistic testing of batteries. With the advent of wide-bandgap power semiconductors in electric vehicle powertrains and the resulting higher switching frequencies, it is necessary to consider also the AC components of the battery current during the testing cells, modules and packs. How much the AC currents actually effects the cell ageing and how much it poses a safety risk due to increased self-heating is still subject to active research. This must be evaluated case-by-case – also with the help of the newly developed set of tools.

4.3 Use Case 3.3

4.3.1 Demonstration

No changes of the use-case/evaluation methodology.

4.3.2 Results and Measurements

The results and measurements of UC3.3 are described in detail in WP4 and WP5. The main results and measurements are briefly summarized as follows.

Based on an extensive measurement campaign on the Fiat500e battery system we can conclude the following findings:

- Testing temperature has only a minor impact on the damage values
- The external excitation has a major impact on the damage, which depends on a lot of factors, e.g. vehicle type, battery position in the vehicle, mounting situation, use case of the vehicle, etc.
- The SOC also has a major impact on the vibration response of the battery module due to the swelling behavior of the battery cells
- The ISO 12405 vibration profile is in a good agreement on global basis
- The vibration response of internal components of the battery system shows a significant energy increase compared to the ISO 12405 profile

From the mentioned results, we conclude a ranking for important factors which should be considered for mechanical safety testing of a battery system:

1. Vibration loads from the street profile/roughness have the major impact to the damage behavior, therefore we highly recommend vehicle measurements to evaluate the load collective.
2. Additionally, we recommend to superimpose a SOC variation during vibration testing, which is currently not considered in the ISO 12405.
3. The temperature variation can be neglected, at least for the considered battery system and the measured positions.

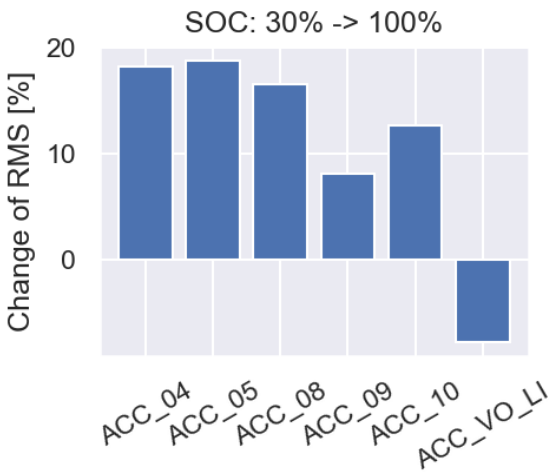

Figure 4-26: Change in RMS with variation of SOC for different measurement positions inside the battery (ACC_04 – ACC_10) and on the mounting position (ACC_VO_LI).

In terms of the mechanical vehicle simulation for vibration loads on the battery system we achieved a very good agreement between simulation and experiment on rough road track. A variety of models were investigated. The

best results were achieved by using a neural network (NN) approach using vibration input data from all three measured direction. The model was also applied to real road excitations to validate the transfer behavior to different street surfaces. The model has difficulties to predict the high frequency response in a standard street environment. The higher loading amplitudes can be well predicted by the model, see in Figure 4-26.

From the simulation results for vibration load data estimation of the battery, we conclude the following lessons learned:

1. The vibration transfer models have to be calibrated for each vehicle. A vehicle specific parameter set cannot be transferred to a different vehicle. Therefore, vehicle measurements are required.
2. The simulation results significantly improve by using all three spatial direction. The agreement between simulation and measurement is reduced by using only the main excitation axis z.
3. Using an artificial intelligence approach (Neural Networks) is very effective and seems to be promising for further applications, see in Figure 4-26.

We see the following impact by using the presented technique for the modeling of vibration transfer path from the road to the battery:

1. A predictive maintenance strategy can be applied in the vehicle by using one acceleration sensor, installed somewhere in the vehicle. Abnormalities in the signals could be an indicator for safety relevant issues on the battery system

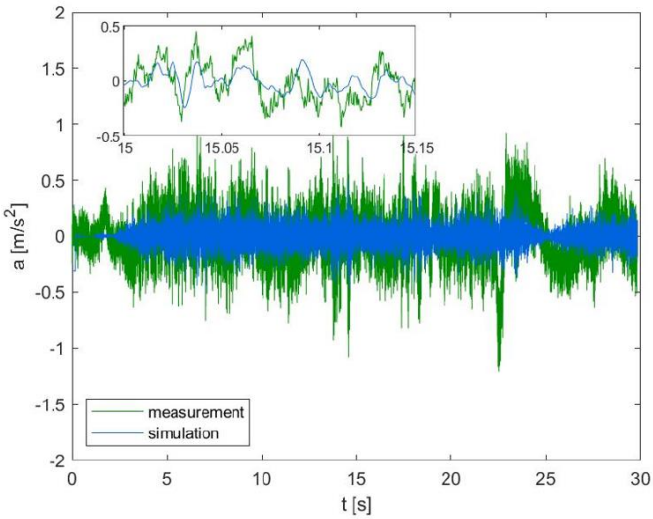

Figure 4-27: Comparison of simulation model prediction and measurement under real road conditions on street around Stuttgart, Germany.

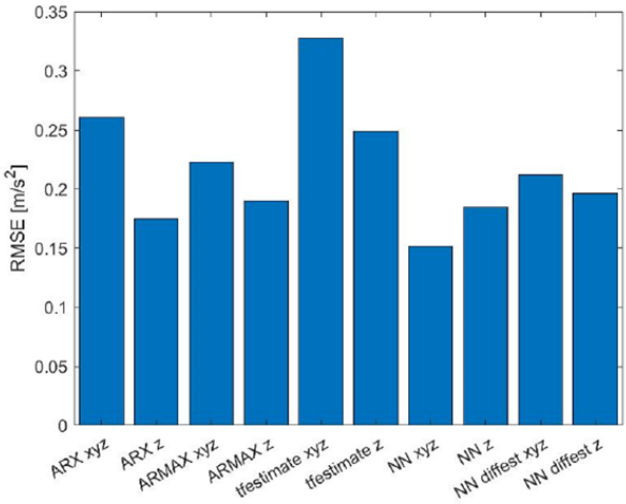

Figure 4-28: Model prediction quality for the used modeling strategies.

4.3.3 Evaluation

The loading energy can be up to 20% higher for different SOC values, see Figure 4-26. The reason for this behavior can be attributed to the swelling behavior of each single battery cell. Consequently, the stiffness of a battery module changes with the variation of SOC. For the considered battery system, the ISO 12405 would be not conservative in terms of SOC, since ISO 12405 recommends to test with 50% SOC. We proclaim a safety improvement of 1.5 by variate the SOC value during vibration testing. This procedure is also closer to the field loading and therefore relevant for all battery systems.

4.3.4 Conclusion

The extensive vibration study of the battery system showed the impact of a wide variety of battery dependent parameters which were not captured before. Some parameters don't have a major impact to the vibration response (e.g. temperature) and other parameters (e.g. road roughness and SOC) have a major impact. The results help to understand the complex behavior of a battery under vibration loading. Furthermore, we could give a list of recommendations for future battery vibration testing to increase the safety.

4.4 Use Case 3.4

Over 10 million vehicles were recalled between 2005-2015 due to SW related issues [1]. The consequence of which, the safety and reliability of the embedded SW has been a major concern for Tier 1 suppliers and automotive manufacturers. Also developing technology brings more complexity in the components of the vehicles. As discussed in D6.1, this complexity comes along with a wide variety of possible failures, which should be managed in the earlier stage of fault occurrence to preserve the safety and prevent the EV from permanent malfunctions during the drive cycle. To address the issues related to the development phase, first list of recommendations was given in Deliverable 5.7 to ensure that electrified road vehicle algorithms conform to the ISO26262 standards. The core of the recommendation was to address the challenges of the cause of the failures during the development process, the subjectivity of the risk analysis techniques, and non-systematic deployment of FMEA. Therefore, a systematic, analytical and objective software development process was introduced.

Moreover, fault-tolerant torque allocation algorithm (TAA) is developed for all wheel drive (AWD) configuration. It is aimed to contribute to safety and speed tracking performance with the hardware redundancy. According to **Error! Reference source not found.**, the reference torque is generated based on driver's demand. In normal condition, this reference torque can be distributed between front and rear EMs according to a predefined fixed ratio or using the energy optimization module. This module can optimize the power consumption online as described in D6.1. For the sake of less computational cost, efficiency map of the whole system is extracted which can be used as an offline look-up optimizer. When a faulty condition happens, optimization is not meaningful anymore since all the optimum front and/or rear torques are not applicable to faulty hardware.

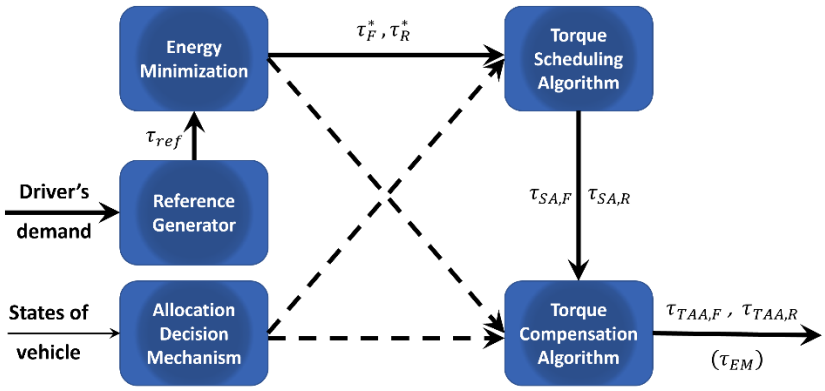

Figure 4-29: AWD Torque Allocation Algorithm (TAA) for e-RT

Therefore, the reference torque is just distributed according to the predefined share for front and rear EMs (corresponding to motors size). However, a constraint optimization using updated EMs maps for new faulty condition would be still implementable which need a wise design. The scheduling algorithm modifies the torque according to the fault. If any of the EMs is in normal working state while the other is faulty, the compensation module tries to add the deducted torque from the faulty EM to the healthy one. So, the TAA output uses the maximum capacity of the AWD e-RT to minimize the fault effect on the driver's expectance.

As discussed, it is aimed to increase the safety using hardware redundancy. Using an additional EM and converting e-RT to AWD configuration will contribute to safety in faulty cases. Main target of the torque transfer is to preserve the speed tracking performance by transferring the deviated torque of faulty EM to the other EM under specific faulty conditions.

4.4.1 Demonstration

No changes of the use-case/evaluation methodology.

4.4.2 Results and Measurements

Vehicle controller-based safety improvement aimed in UC 3.4. In order to achieve the aim, Ford Otosan supported the use case under following tasks:

- Safety test case specification
- Integrated vehicle model updates to perform safety tests.
- State diagrams of high voltage components were defined for control model development.
- Requirement for start-up and shutdown sequence defined
- Safe operating areas for e-motor and battery system are defined.

Collaboration between US and FO under UC3.4 tasks were shared in Figure 4-30 below.

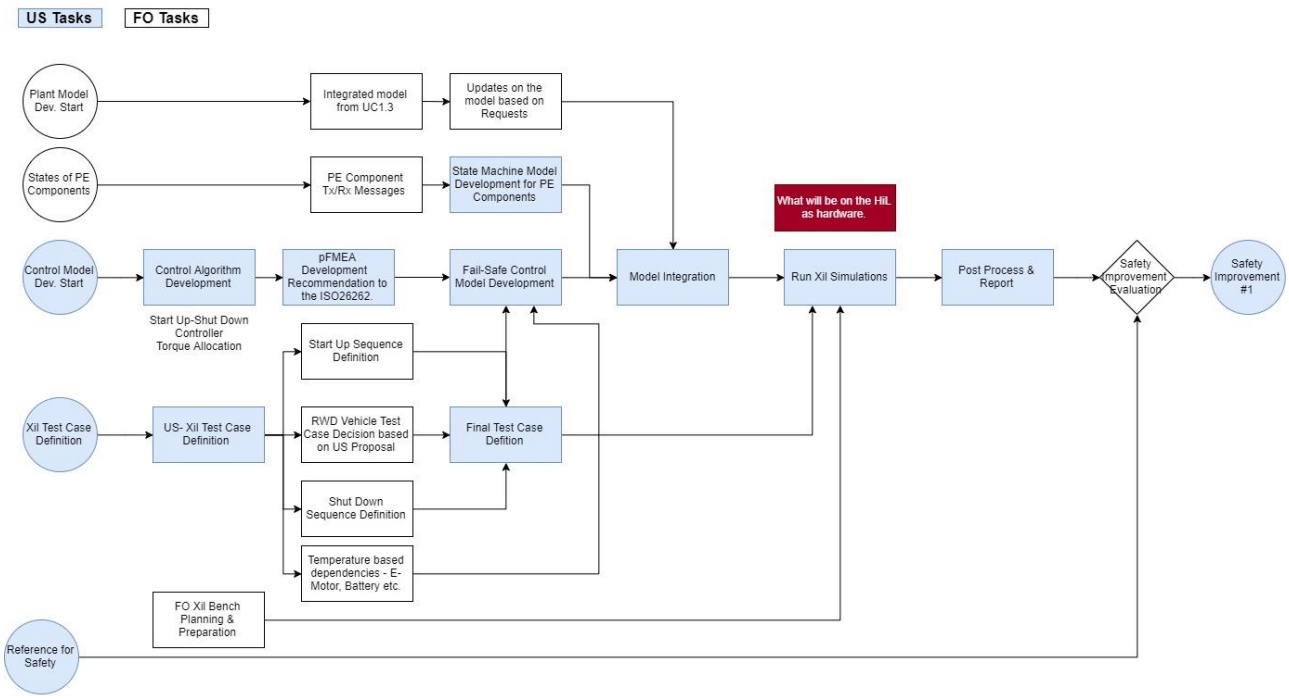

Figure 4-30: UC 3.4 Workflow & Responsiblities

4.4.2.1 Safety Test Cases

In order to validate the safety functions, several test cases for e-motor and battery system were designed and failure scenarios related to cause were listed as below:

- Reduced performance due to electric machine or high voltage battery temperature failure
- Shutdown due to electric machine or high voltage battery temperature failure
- Reduced performance and then shutdown due to electric machine or high voltage battery temperature failure
- Shutdown due to communication error

- **E-Motor Xil Test Cases**

Test Case 1: This test case related with electric motor temperature. If electric motor temperature is between the reduced performance temperature threshold and maximum temperature for shutdown ($T_{EMRP} < T_{EM} <$

$T_{EM_{MAX}}$), vehicle performance reduction is expected. This situation can occur at the beginning or during the drive cycle.

Test Case 2: This test case related with electric motor temperature. If electric motor temperature is higher than maximum allowed temperature ($T_{EM} \geq T_{EM_{MAX}}$), error flag shall be raised by decision-making blocks and control algorithm shall shutdown the vehicle. This situation can occur at the beginning or during the drive cycle.

Test Case 3: This test case related communication fault between the motor controller and supervisory control unit. If there is a communication fault, software shall raise error flag and shutdown sequence shall be activated. This situation can occur at the beginning or during the drive cycle.

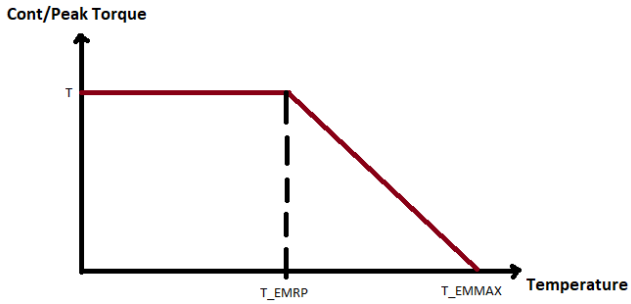

Figure 4-31 :Torque derating due to electric motor temperature

- **Battery Xil Test Cases**

Test Case 4: This test case is related with battery temperature. If the battery temperature is between the battery reduced performance temperature and battery maximum allowed temperature range ($T_{BRP} < T_B < T_{B_{MAX}}$), performance reduction of the vehicle is expected. This situation can occur at the beginning or during the drive cycle.

Test Case 5: This test case is related with battery temperature. If battery temperature is higher than maximum allowed temperature ($T_B \geq T_{B_{MAX}}$), all error flags shall be raised by decision-making block and control algorithm shall shutdown the vehicle. This situation can occur at the beginning or during the drive cycle.

Test Case 6: This test case is related communication fault between the battery management system and supervisory control unit. If there is a communication fault, software shall raise error flag and shutdown sequence shall be activated. This situation can occur at the beginning or during the drive cycle.

4.4.2.2 Integrated Vehicle Model

Main tasks for integrated vehicle model are completed in UC 1.3 and reported under D6.1. For UC3.4, this reference model was updated based controller requirements, which were shared by US. Electric motor available torque predicted added to the model based on heat capacity of the system. Current limitations of the battery were also added based on available energy capacity and cell temperature prediction. Apart from these, metrics listed in Table 4-1 were also implemented to the model.

Table 4-1: Controller Requirement Based Signal Updates

Variables	Name	I/O	Type	Unit	Dimension
Overwrite torque	TorqueOverwrite	Input	Physical	Nm	1
Overwrite desired current	CurrentOverwrite	Input	Physical	A	1
Thermal capacity value	Thermal Indicator	Output	Physical	%	1

Torque output calculation was also modified in the e-motor model. Desired torque was function of road load and reference speed at the beginning where only limitation was the mechanic torque limit of the e-motor. In the new model, a thermal indicator value was implemented where e-motor heat capacity is normalized. Based on the value of this metric, available torque was limited. Process flow defined in Figure 4-32.

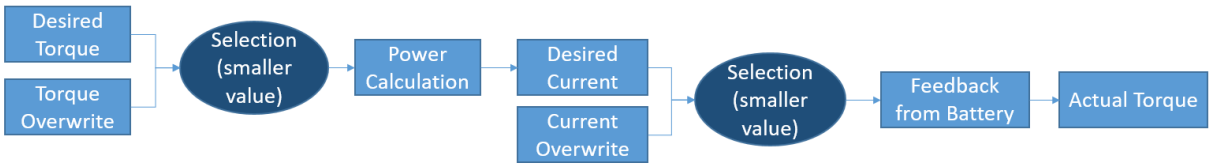

Figure 4-32 : Torque Path

As in the Table 4-2, if the e-motor speed is less than the normalized reference 1 and the thermal indicator is less than 80% of the torque output is not limited. If the thermal indicator reaches to 95% and the e-motor speed is greater than 1 than the available torque shall be limited to '0' Nm. The E-motor speed and thermal indicator values between the given limits can be designed according to the control algorithm.

Table 4-2: Torque Limits According To Thermal Indicator

	Unit	100% Torque Value	0% Torque Point
Speed	RPM	<= 1*	> 1*
Thermal Indicator – Stator & Rotor	%	< 80	> 95

4.4.2.3 Component States

Plant models for an integrated vehicle model was derived from an UC1.3 reference model and controller models were developed from scratch for UC3.4. In order to perform accurate modelling of the component, the controller state diagrams for each component has been defined. Component controller models have two message types in principle. One of them is the receive messages (RX); the other one is the transmitting messages (TX). The RX messages are the ones that components are getting from the supervisory control unit and the TX messages are the ones that each component is broadcasting to CAN network. The controller model shall send RX messages to control and change component states. In order to confirm the state changes and control algorithm, the TX messages can be examined.

Table 4-3: Battery System Signals

Module	Type	Signal	Units / States
BMS	RX	Battery Use Signal	1/0
		Isolation Disable Signal	1/ 0
	TX	Main State 1	Initialization / Standby / Precharge / Operational / Error
		Main State 2	1 / 0

Table 4-4 : e-Drive **System Signals**

Module	Type	Signal	Units / States
MCU	RX	OperationRequest	Standby / OperationalReq / ShutdownReq
		CommandMode	TorqueMode / SpeedMode
		Operational ModeCmd	Neutral / EV
	TX	Operational Mode	Neutral / EV

		MCU Main States	Initialisation / Standby / StartUp / TearDown / Operational / Failure / CloseDown / ReadyToShutDown / WaitForCooling

Table 4-5: Power Take-Off System Signals

Module	Type	Signal	Units / States
PTO	RX	Control Signal	Initialize / Energise / Shutdown / NoCommand / Enable / FaultReset / ActiveShort
	TX	Inverter Status Signal	None / Not ready to switch on / Shutdown / Precharge / Energized / Enabled / FaultOff

4.4.2.4 Shutdown Sequences

The supervisory control unit software (E-VCU) must control systems in the interfaces and enable safe shutdown of the high voltage DC-bus and safe discharge of high voltage from the system. The E-VCU hardware shall control power electronics parts in the system through the CAN network, resistors and contactors either by CAN or hardwired. The E-VCU hardware interfaces are shared as in Figure 4-33.

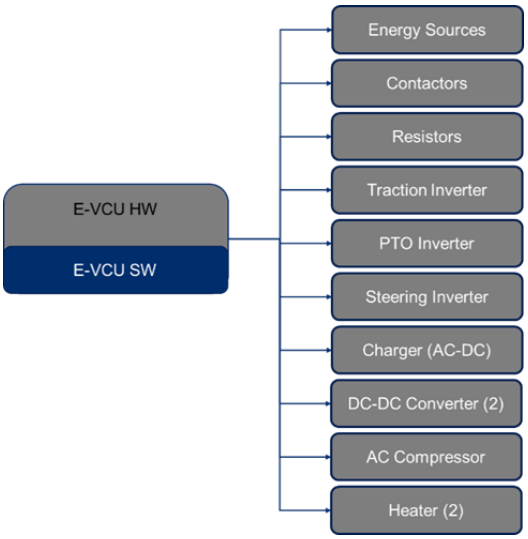

Figure 4-33: E-VCU hardware Interface

The following sequence is defined for safe shutdown of the vehicle and the requirement are defined as below:

1. Vehicle safe shutdown event shall be triggered by either driver event or AC charge complete/stop request.
2. In order to start the shutdown of the system e-VCU shall monitor the vehicle speed and enable shutdown process if the vehicle speed is below X (calibratable) km/h.
3. If shutdown sequence triggered, e-VCU shall disable all HV components.
4. E-VCU shall disabled HV battery by CAN message through state change (to 'standby' mode).
5. E-VCU shall monitor battery state. Standby is expected, in any other state e-VCU shall raise error flag.
6. E-VCU shall disable HV system (vehicle) isolation through CAN communication.
7. E-VCU shall enable battery isolation monitoring through CAN communication.
8. E-VCU shall request battery contactor to open through CAN communication.
    a. Contactors in the system are shared in Figure 4-34. Battery contactor positive and contactor negative to be opened one time step later from the E-VCU request.
9. E-VCU shall enable discharge resistor relay through hardwire.
    a. K3 contactor to be closed shared in Figure 4-35.
    b. System shall be discharged in 1 second.

10. E-VCU shall open other contactors (K4-K5).
11. All system shall go to sleep mode after shutting down if no other event triggered.

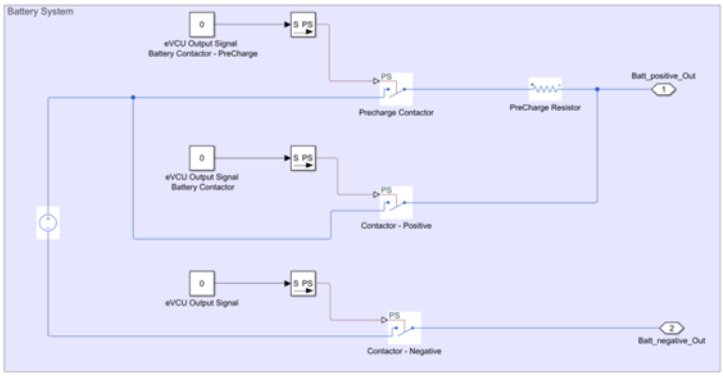

Figure 4-34: Battery contactors and pre-charge circuit

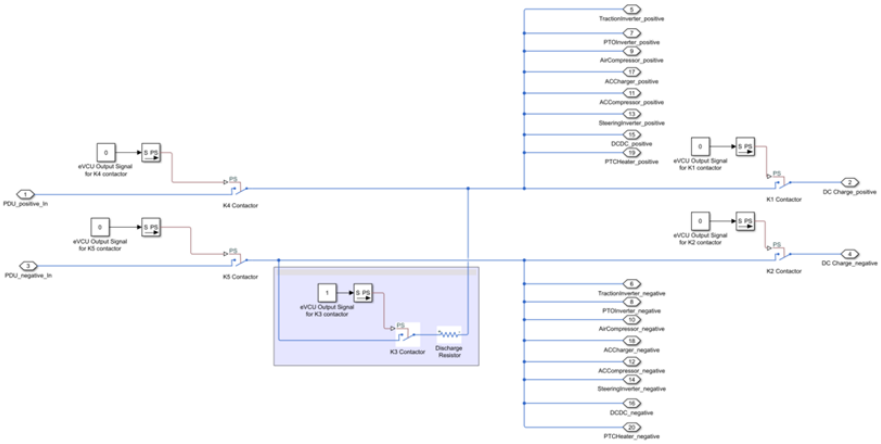

Figure 4-35 : Contactor locations on high voltage network

4.4.2.5 Start-Up Sequence

Following sequence was defined for safe start-up of high voltage system.

1. Vehicle start-up sequence shall be triggered by driver event (turn the ignition key/switch to KL15 position).
2. Battery management system (BMS) and traction motor control unit (MCU) shall broadcast their status as 'Standby'.
3. System isolation monitoring device shall measure system isolation and share the results with e-VCU.
4. E-VCU shall check interlock current and broadcast HVIL OK.
5. E-VCU shall control system error messages and if no error available, at this point HV system is ready to start up.
6. If ignition switch is at start position for greater 1 second and brake pedal is pressed at the same time;
    a. E-VCU shall transmit KL50 signal.
    b. E-VCU shall transmit "battery enable" signal to the BMS.
7. If battery enable signal is received by BMS;
    a. BMS shall transmit its status as 'Precharge' within less than 1 second.
    b. BMS system shall close battery negative contactor within less than 1 second.
    c. BMS shall close its precharge contactor within less than 1 seconds.
    d. If system voltage (at PE component side) rises above 95% of the battery system voltage, battery shall change 'Battery_precharge' value from '0' to '1'.

e. BMS shall close battery positive contactor within less than 1 second.
f. BMS state shall be changed to 'Operational' mode.
g. BMS shall change Battery_precharge' value from '1' to '0'.
h. Battery shall open the precharge contactor within 1 second.

8. DCDC unit shall transmit unit enable signal through CAN.
9. If parking brake switch position and gear level is changed by the driver, traction motor control unit shall change its state to 'Operational' from Standby.
10. E-VCU shall activate system components (Power electronic components especially) based on components activation strategy.
    a. Steering inverter shall be activated once handbrake switch released within less than 1 second.
11. If failure happens at any step of the mechanism then e-VCU shall raise error flag and prevent start up.

Flexible-Safe Shutdown Sequence Controller

The aim is to develop Safe shutdown sequence control (SDSC) algorithm with consideration of various functional and safety requirements for the Ford Otosan refuse tuck (e-RT). The software should enable a safe shutdown of the e-RT that consists of high voltage bus, while monitoring the discharge status of the high voltage system, as well as other high voltage components. A safe shutdown refers to the sending of closing command to the HV system in the required sequence and monitoring the drop of the high voltage bus below 60-volt DC. In order to design and develop the SDSC software, a rule based methodology was generated as shown in Figure 4-36, wherein an in-depth literature review along with human expertise, lead to the development of a software requirement specification (SRS) document that specifies the shutdown of FO e-RT in a sequential order. In other words, the SRS acts as cluster of requirements which includes i) functional, ii) non-functional, iii) safety, iv) product function, v) external interface, vi) performance, vii) operating environment, viii) maintainability and ix) quality requirements. Using the MATLAB Simulink©, the SDSC was modelled and developed. Based on the conditions evaluated from the SRS, negative test cases were generated and using the Software Fault Injection technique, Model-in-the-Loop (MiL) tests were carried out. To know, whether the developed solution performs with respect to the user needs, requirement tracing was carried out. Once the requirements as mentioned in the SRS are achieved, the software developed is successful. To carry out the MiL tests, various scenarios for AWD configuration were developed as shown in Table 4-6.

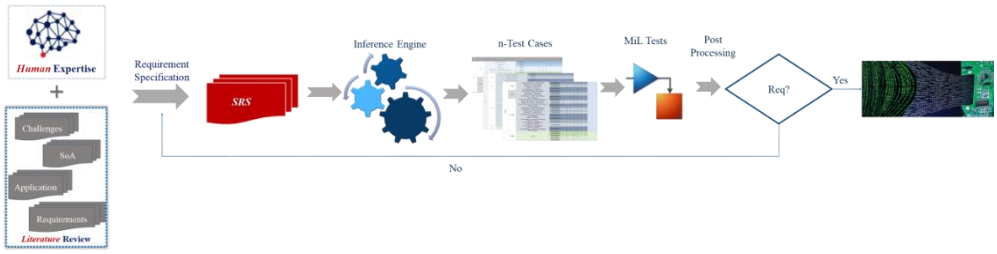

Figure 4-36: Safe Shutdown Sequence Controller Methodology

S2FEMS0REM/X: $(T_{FEM} \geq T_{FEMmax}) \wedge (T_{REM} < T_{REMRP})$

The scenario is presented when the vehicle is in motion, therefore, in Figure 4-37 i) the KeyON signal means that the vehicle is powered by the high-voltage battery, and Figure 4-37 ii) shows that the vehicle is not in charging mode (charging cable is not connected). In the Figure 4-37 iv), it can be seen that the Temperature of the front electrical machine (FEM) is higher than the maximum temperature limit while the temperature of the rear electrical machine is in normal condition Figure 4-37 v). In this case, the SDSC sends an activation commands to torque allocation algorithm (TAA) Figure 4-37 vi). It should be noted that, the battery contactors are still closed,

which means that vehicle is not sent to shutdown. Therefore, this shows that the load on the FEM is zero, while on the REM is 100%, making the system fault tolerant.

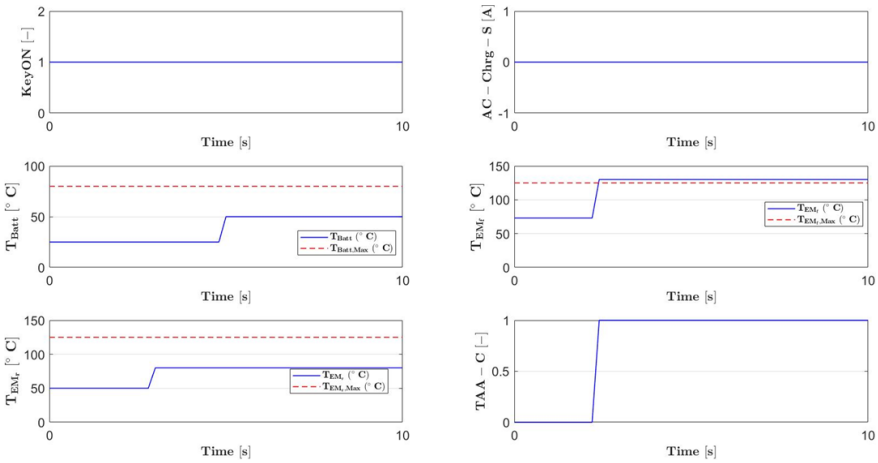

Figure 4-37: i) Key On, ii) AC charging, iii) temperature of the battery, iv) front electrical machine temperature, v) rear electrical machine temperature, vi) torque allocation algorithm activation command

S0FEMS2REM/X: (T_{FEM}<T_{FEMRP}) ∧ (T_{REM}≥T_{REMmax}):

The scenario is presented when the vehicle is in motion, therefore, in Figure 4-38: i) the KeyON signal which means that the vehicle is powered by the high-voltage battery, and Figure 4-38: ii) shows that the vehicle is not in charging mode (charging cable is not connected). In the Figure 4-38: v), it can be seen that the temperature of the REM is higher than the maximum temperature limit while the temperature of the FEM is in normal condition (Figure 4-38: iv). In this case, the SDSC sends an activation commands to torque allocation algorithm (TAA) Figure 4-38: vi). It should be noted that, the battery contactors are still closed, which means that vehicle is not sent to shutdown. Therefore, this shows that the load on the REM is zero, while on the FEM is 100%, making the system fault tolerant.

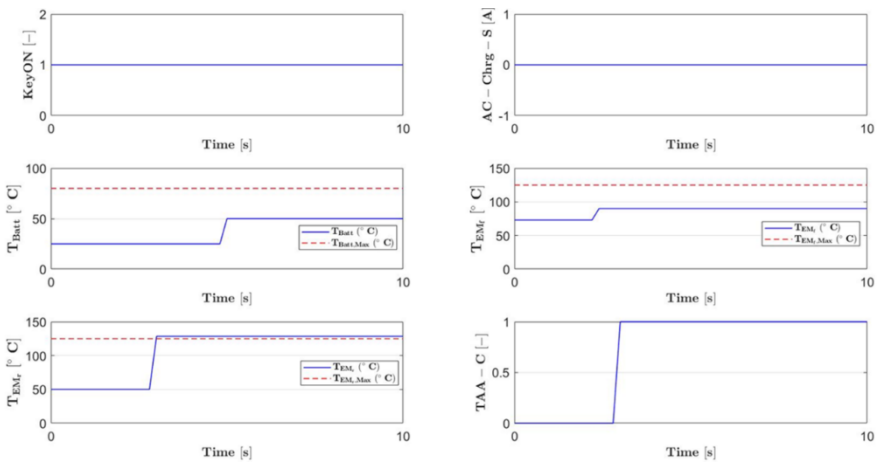

Figure 4-38: i) Key On, ii) AC charging, iii) temperature of the battery, iv) front electrical machine temperature, v) rear electrical machine temperature, vi) torque allocation algorithm activation command

S2FEMS2REM/X: (T_{FEM}≥T_{FEMmax}) ∧ (T_{FEM}≥T_{FEMmax}):

The scenario is presented when the vehicle is in motion, therefore, in Figure 4-39 i) the KeyON signal means that the vehicle is powered by the high-voltage battery, and Figure 4-39 ii) shows that the vehicle is not in charging

mode (charging cable is not connected). In the Figure 4-39 iv) and Figure 4-39 v), it can be seen that the temperature of the FEM and REM is higher than the maximum temperature limit respectively. In this case, the SDSC shuts down the complete vehicle as both the EMs has abrupt temperature failure. It should be noted that, the battery contactors are opened, which means that vehicle is sent to shutdown state Figure 4-39 vii) and Figure 4-39 viii).

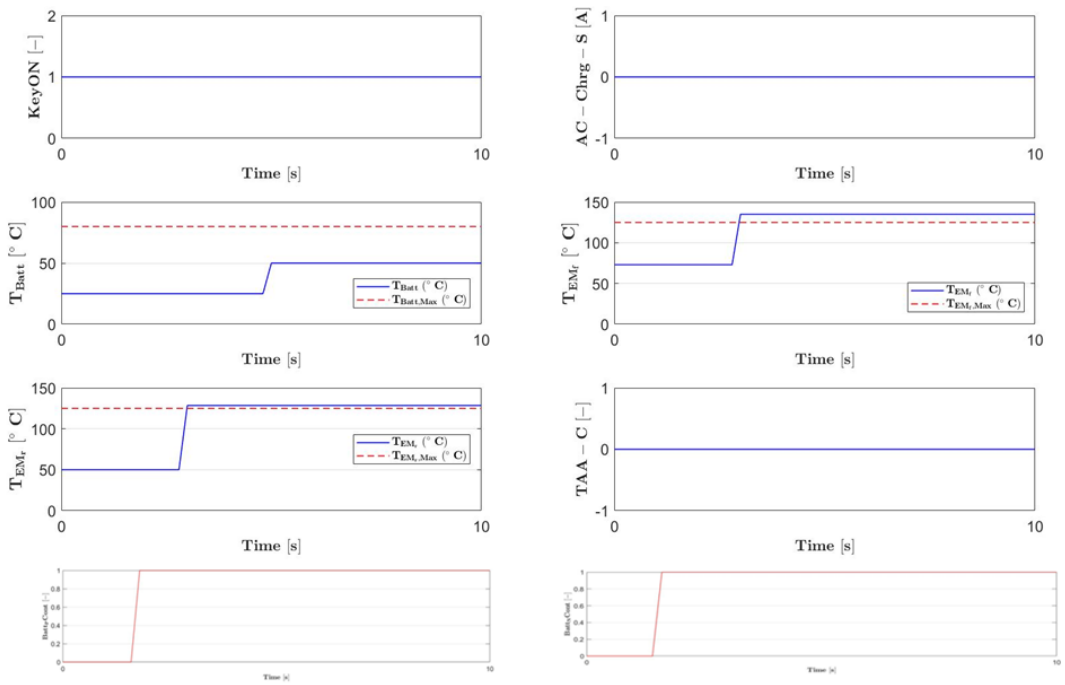

Figure 4-39: i) Key On, ii) AC charging, iii) temperature of the battery, iv) front electrical machine temperature, v) rear electrical machine temperature, vi) torque allocation algorithm activation command, vii) positive battery contactor and viii) negative battery contactors

Fault Tolerant Algorithm

Referring to Pries [2], FMEA is defined and introduced in D6.1 for RWD e-RT. For AWD e-RT, it is not necessary to change the FMEA given for RWD since failure modes are still the same. The corresponding test cases for AWD configuration are given in Table 4-6.

Table 4-6 Test scenarios for AWD EV configuration

Fault Source	Failure Cause	Scenarios	TA	SDSC	SSC
FEM	$(T_{FEMRP} < T_{FEM} < T_{FEMmax}) \wedge (T_{REM} < T_{REMRP})$	S1FEMS0REM/XY	✓	-	-
	$(T_{FEM} \geq T_{FEMmax}) \wedge (T_{REM} < T_{REMRP})$	S2FEMS0REM/X	✓	-	✓
	$(T_{FEM} \geq T_{FEMmax}) \wedge (T_{REM} < T_{REMRP})$	S2FEMS0REM/Y	✓	✓	-
	$(T_{FEMRP} < T_{EM} < T_{FEMmax}) \rightarrow (T_{FEM} = T_{FEMmax}) \wedge (T_{REM} < T_{REMRP})$	S3FEMS0REM/XY	✓	✓	-
REM	$(T_{FEM} < T_{FEMRP}) \wedge (T_{REMRP} < T_{REM} < T_{REMmax})$	S0FEMS1REM/XY	✓	-	-
	$(T_{FEM} < T_{FEMRP}) \wedge (T_{REM} \geq T_{REMmax})$	S0FEMS2REM/X	✓	-	✓
	$(T_{FEM} < T_{FEMRP}) \wedge (T_{REM} \geq T_{REMmax})$	S0FEMS2REM/Y	✓	✓	-
	$(T_{FEM} < T_{FEMRP}) \wedge (T_{REMRP} < T_{REM} < T_{REMmax}) \rightarrow (T_{REM} = T_{REMmax})$	S0FEMS3REM/XY	✓	✓	`-
F∧REM	$(T_{FEMRP} < T_{FEM} < T_{FEMmax}) \wedge (T_{REMRP} < T_{REM} < T_{REMmax})$	S1FEMS1REM/XY	✓	-	-

	$(T_{FEMRP} < T_{FEM} < T_{FEMmax}) \wedge (T_{REM} \geq T_{REMmax})$	S1FEMS2REM/X	✓	-	✓
	$(T_{FEMRP} < T_{FEM} < T_{FEMmax}) \wedge (T_{REM} \geq T_{REMmax})$	S1FEMS2REM/Y	✓	✓	-
	$(T_{FEMRP} < T_{FEM} < T_{FEMmax}) \wedge$ $(T_{REMRP} < T_{REM} < T_{REMmax}) \rightarrow (T_{REM} = T_{REMmax})$	S1FEMS3REM/XY	✓	✓	-
	$(T_{FEMRP} < T_{FEM} < T_{FEMmax}) \wedge C_{REM}$	S1FEMS4REM/XY	✓	✓	
	$(T_{FEM} \geq T_{FEMmax}) \wedge (T_{REMRP} < T_{REM} < T_{REMmax})$	S2FEMS1REM/X	✓	-	✓
	$(T_{FEM} \geq T_{FEMmax}) \wedge (T_{REMRP} < T_{REM} < T_{REMmax})$	S2FEMS1REM/Y	✓	✓	
	$(T_{FEM} \geq T_{FEMmax}) \wedge (T_{FEM} \geq T_{FEMmax})$	S2FEMS2REM/X	-	-	✓
	$(T_{FEM} \geq T_{FEMmax}) \wedge (T_{FEM} \geq T_{FEMmax})$	S2FEMS2REM/Y	-	✓	
	$(T_{FEM} \geq T_{FEMmax}) \wedge$ $(T_{REMRP} < T_{REM} < T_{REMmax}) \rightarrow (T_{REM} = T_{REMmax})$	S2FEMS3REM/XY	✓	✓	✓
	$(T_{FEMRP} < T_{EM} < T_{FEMmax}) \rightarrow (T_{FEM} = T_{FEMmax}) \wedge$ $(T_{REMRP} < T_{REM} < T_{REMmax})$	S3FEMS1REM/XY	✓	✓	-
	$(T_{FEMRP} < T_{EM} < T_{FEMmax}) \rightarrow (T_{FEM} = T_{FEMmax}) \wedge$ $(T_{REM} \geq T_{REMmax})$	S3FEMS2REM/X	✓	✓	✓
	$(T_{FEMRP} < T_{EM} < T_{FEMmax}) \rightarrow (T_{FEM} = T_{FEMmax}) \wedge$ $(T_{REM} \geq T_{REMmax})$	S3FEMS2REM/Y	✓	✓	-
	$(T_{FEMRP} < T_{EM} < T_{FEMmax}) \rightarrow (T_{FEM} = T_{FEMmax}) \wedge$ $(T_{REMRP} < T_{REM} < T_{REMmax}) \rightarrow (T_{REM} = T_{REMmax})$	S3FEMS3REM/XY	✓	✓	-
F∧REM	$C_{F \wedge REM}$	S4FEMS0REM/X	✓	-	-
		S0FEMS4REM/X	✓	-	-
		S4FEMS4REM/X	-	-	✓
		S4FEMS0REM/Y	✓	-	-
		S0FEMS4REM/Y	✓	-	-
		S4FEMS4REM/Y	-	✓	-
Battery	$(T_{BRP} < T_B < T_{Bmax})$	S1B/XY	✓	-	-
	$(T_B \geq T_{Bmax})$	S2B/X	-	-	✓
	$(T_B \geq T_{Bmax})$	S2B/Y	-	✓	-
	$(T_{BRP} < T_B < T_{Bmax}) \rightarrow (T_B = T_{Bmax})$	S3B/Y	✓	✓	-
	C_B	S4B/X	-	-	✓
		S4B/Y	-	✓	-

For investigating the performance of the TA algorithm on all-wheel drive EV, all test scenarios are simulated by MATLAB/Simulink. To prove satisfactory performance of the TAA, results of simulation for selected test cases from Table 4-6 are presented in this section. To better understand the action of TAA to each EM, reader can refer to D6.1 which describes what happens to EM torque in details. Here, the hardware redundancy and torque compensation characteristic of TAA is more focused on. NREL drive cycle is used for simulations.

Test Case 1: S1FEMS1REM/ XY

Situation: Reduced performance in both front and rear EMs at start-up or during drive

Reason: $(T_{FEMRP} < T_{EM} < T_{FEMmax}) \wedge (T_{REMRP} < T_{REM} < T_{REMmax})$

According to Figure 4-40 : and Figure 4-41, EMs temperature in this test case fall in the reduced performance region for some time. In these time intervals torque moderation flag is activated. According to figures, before t=70s and before t=50s rear and front EMs temperatures are within reduced performance interval and torque moderation flag is activated (ON) by TAA algorithm. In this regions TAA reduces the reference torque to the percentage shown in the right plots.

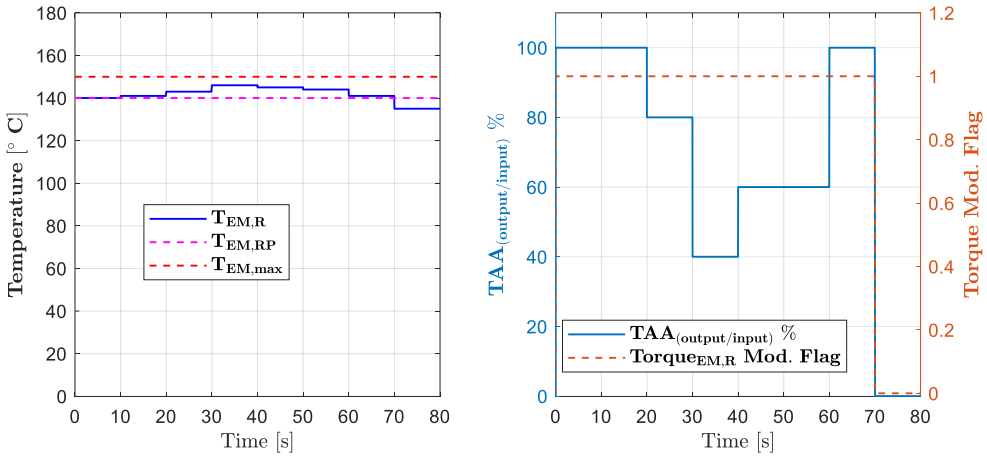

Figure 4-40 : Rear EM temperature profile (left) and TAA action (right)

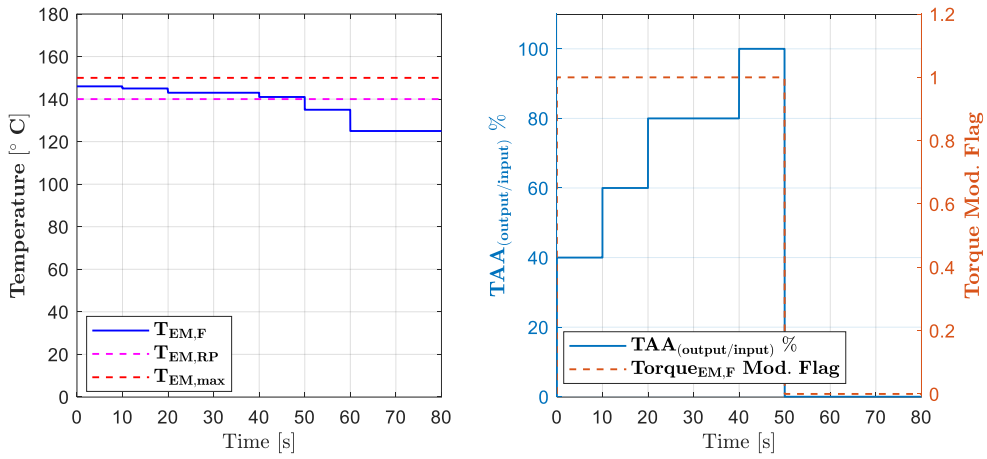

Figure 4-41 : Front EM temperature profile (left) and TAA action (right)

Figure 4-42 and Figure 4-43 shows the reference and moderated torque values by TAA algorithm implementation. As discussed in D6.1, the reference torque is the amount required by the driver action from an EM experiencing no fault. When a temperature fault occurs, it is considered in the reference torque generation by considering the maximum EM capacity at working temperature. Therefore, the driver required torque, which is not plotted here, is always greater than or equal to the reference torque shown in the figure. According to the manufacturer advice, the TAA modifies the plotted reference torque to maintain the EM health and resolve the faulty condition. From the figures the vehicle never uses the maximum available torque (blue) when temperature is over 140°C.

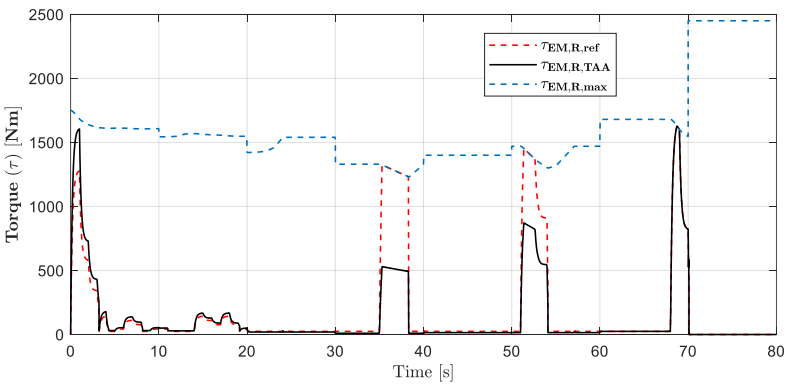

Figure 4-42 :Rear EM reference torque (red) moderated torque (black) with TAA

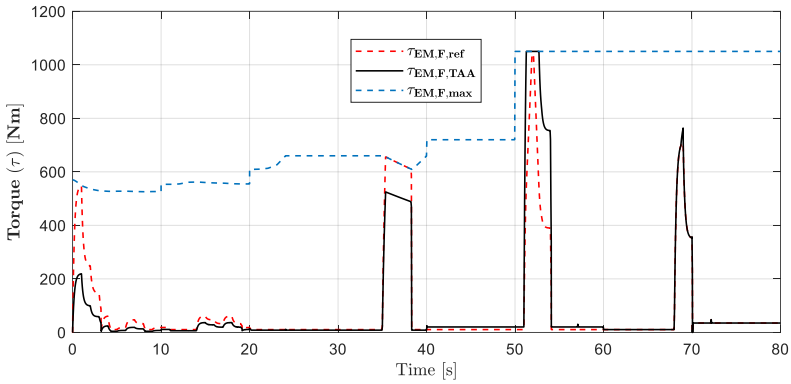

Figure 4-43 :Front EM reference torque (red) moderated torque (black) with TAA

At times in both figures when the applied torque (black curve) is more than the reference torque (red curve); the compensation algorithm is activated and tries to use up to maximum resources to track the driver's intention. It happens at the beginning of the drive for rear EM and at 40s<t<60s for the front EM. It is clearly distinguishable that the compensation is activated when one EM faces a fault and the other is in normal condition.
The resulting speed profile of AWD e-RT is given in Figure 4-44. As seen from the speed profile, the e-RT tracks the speed profile when a few torque is needed, there is no fault. Tracking error is noticeable only when both EMs face fault and high acceleration exist at the same time. Readers could well track what is happening to the EV by comparing all figures of the simulation at any time.

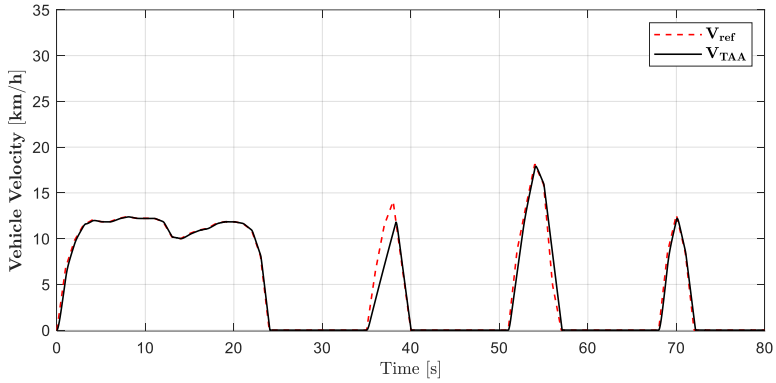

Figure 4-44 :Vehicle reference velocity (red) moderated velocity (black)

This scenario is simulated again while the TAA is inactive to investigate the TAA algorithm effectiveness. As seen in Figure 4-45 the vehicle applies the reference torque to the EM since the TAA is not working (black curve lies on red one). This reference torque in some periods is the maximum available torque of the EM which would be refused if the TAA was active. The same story happens for the front EM as seen in Figure 4-46.

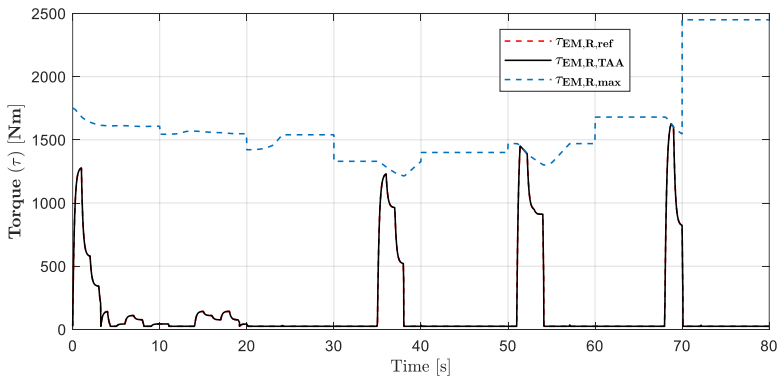

Figure 4-45: Rear EM torque (TAA OFF)-reference torque (red), moderated torque (black) and max available torque(blue)

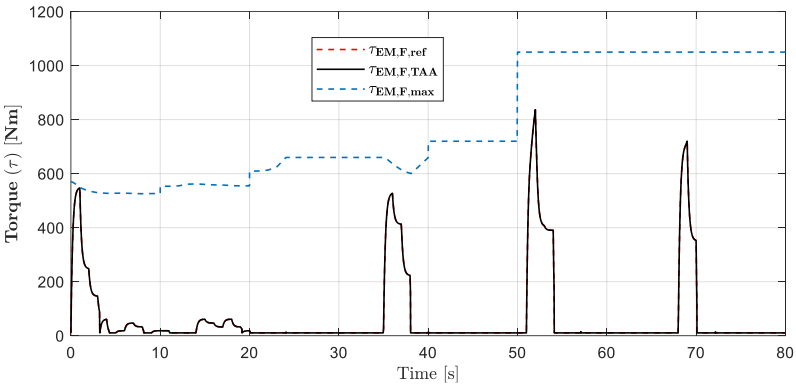

Figure 4-46: Front EM torque (TAA OFF)-reference torque (red), moderated torque (black) and max available torque(blue)

According to Figure 4-47, the reference velocity in this scenario is almost tracked when the TAA is inactive. The penalty, however, is the risk of possible failure to the EMs by applying the maximum available torque at high temperatures. It should be noted that when the TAA is OFF the compensation capability is inactive as well. So, if a motor capacity is reduced due to temperature issues, and high torque is needed at the same time, the other EM does does not compensate the torque. This situation happens twice around t=50s and t=70s when the rear EM is applying its maximum deliverable torque.

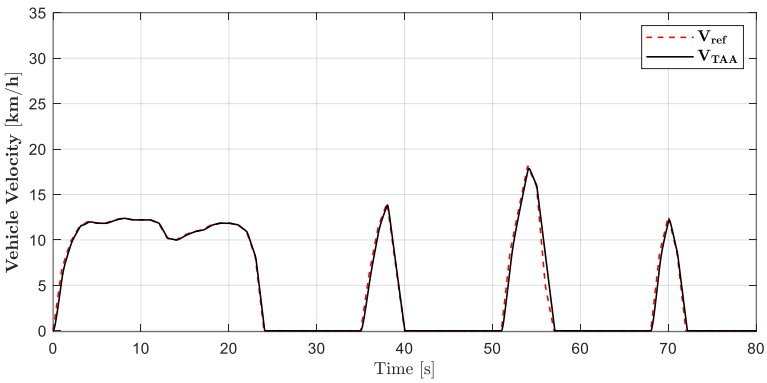

Figure 4-47: Vehicle velocity (TAA OFF)- reference velocity (red) moderated velocity (black)

Test Case 2: S1FEMS3REM / XY

Situation: Reduced performance and shutdown in rear EM and reduced performance in front EM at start-up or during drive

Reason: $(T_{FEMRP} < T_{EM} < T_{FEMmax}) \wedge (T_{REMRP} < T_{REM} < T_{REMmax}) \rightarrow (T_{REM} = T_{REMmax})$

In this test case, the rear EM is under reduced performance resulting in a shutdown as given in Figure 4-48. After t=20s, the rear EM temperature is within reduced performance limits and it exceeds the critical temperature at t=250s which results in shutdown operation (Figure 4-50).

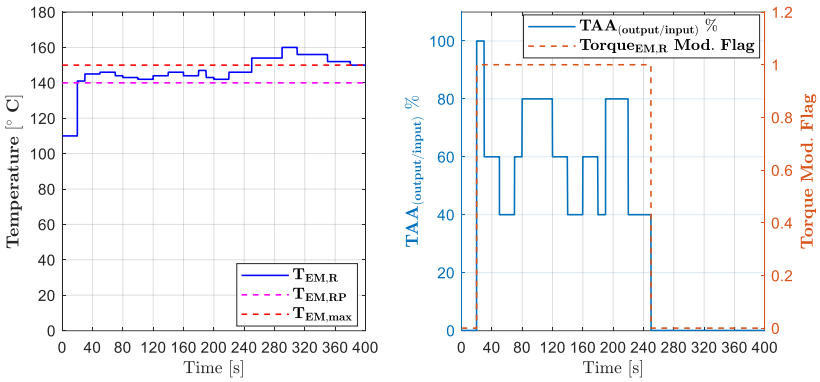

Figure 4-48: Rear EM temperature profile (left) and TAA action (right)

Figure 4-49 shows the temperature change of the front EM. As seen from the figure, the front EM temperature is within the reducing performance limits in the different time instants of the simulation. In the reduced performance region torque moderation the flag is ON and the TAA changes the reference torque according to right plots of Figure 4-48 and Figure 4-49.

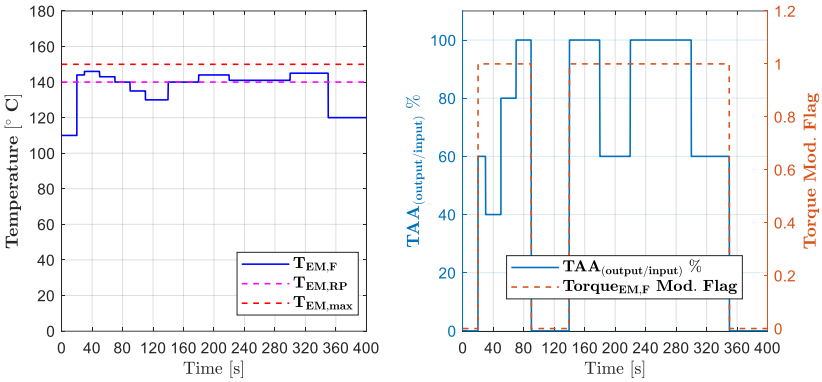

Figure 4-49: Front EM temperature profile (left) and TAA action (right)

Figure 4-50 represents the rear EM communication fault and the shutdown flags. As seen from the figure, th shutdown flag is activated since the EM temperature exceeded the critical temperature at t=250s.

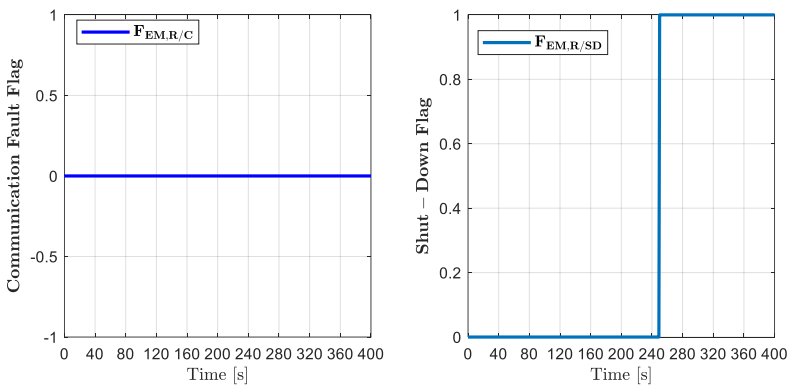

Figure 4-50: Rear EM communication fault flag status (left) and shutdown flag status (right)

Figure 4-50 and Figure 4-51 show the reference and the moderated torque values after the TAA algorithm implementation. Clearly, the vehicle does not use the maximum available torque (blue) when the temperature is some over 140°C. Note that, after t=250s, the torque is not implementable in the rear EM due to shutdown. The

torque compensation happens when the front EM has a capacity more than its reference demanded torque (black curve over red one in Figure 4-52 for 80<t<180s and some of 220s<t<300s).

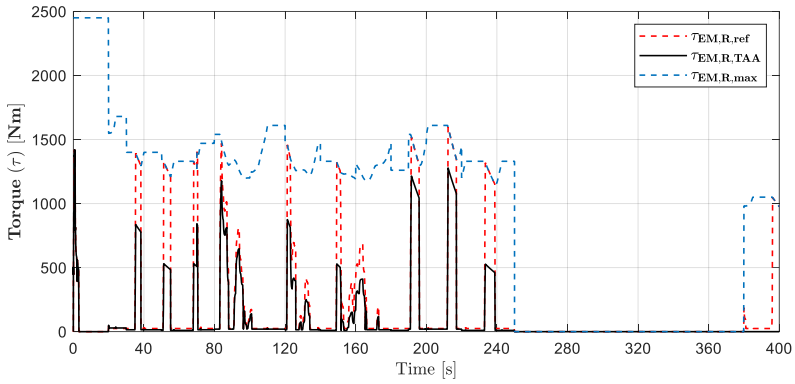

Figure 4-51: Rear EM reference torque (red) moderated torque (black) with TAA

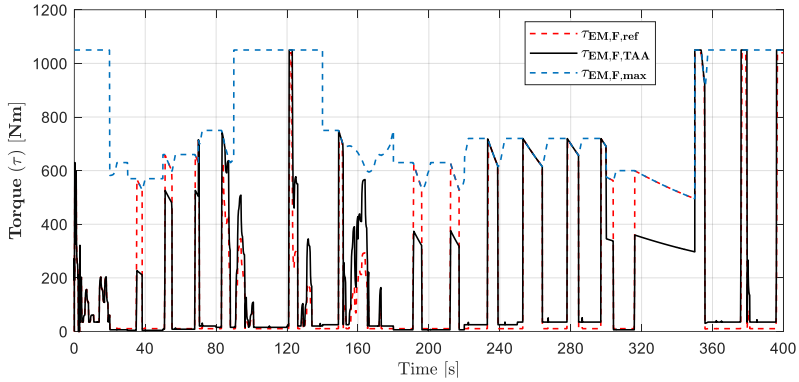

Figure 4-52: Front EM reference torque (red) moderated torque (black) with TAA

The resulting speed value of the e-RT corresponding to the moderated torques is presented in Figure 4-53. As seen from the plot, the reference speed tracking performance is satisfactory until t=250s specially when the torque transfer between motors is implemented. After t=250s, due to the rear EM shutdown torque, lower capacity of the front EM and its own faulty state; the speed tracking performance decreases.

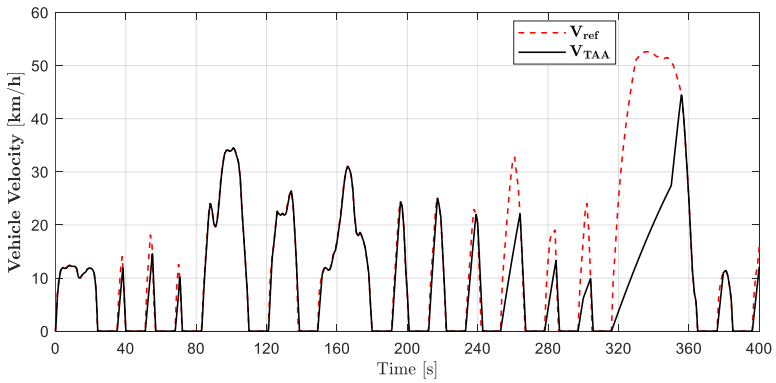

Figure 4-53: Vehicle velocity- reference velocity (red) moderated velocity (black)

Again, this scenario is simulated while the TAA is inactive. As seen in Figure 4-54 the vehicle applies the reference torque to the EM since the TAA is not working (black curve lies on red one). The rear EM in some cases is applying its maximum capacity that can be harmful to it. It is assumed that the rear EM is shutdown by some means when

temperature is over 150℃ . Otherwise a failure may be expected which is not considered in the simulation. A similar situation in applying maximum capacity torque exists for the front EM as well according to Figure 4-55.

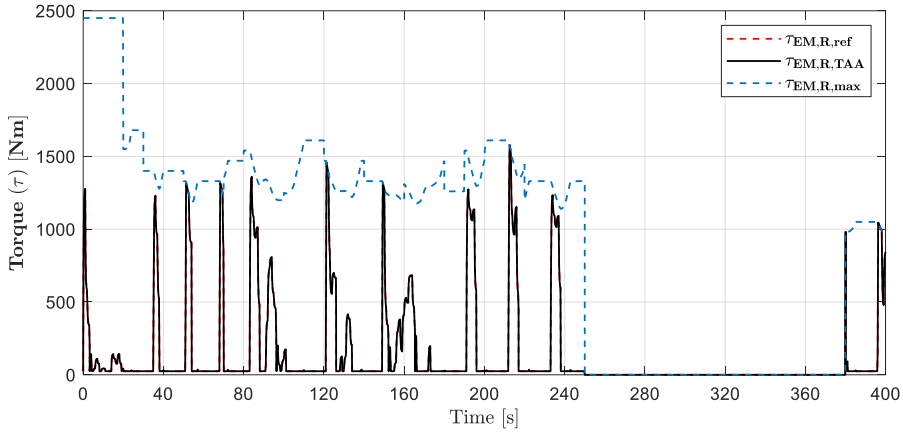

Figure 4-54: Rear EM torque (TAA OFF)-reference torque (red), moderated torque (black) and max available torque(blue)

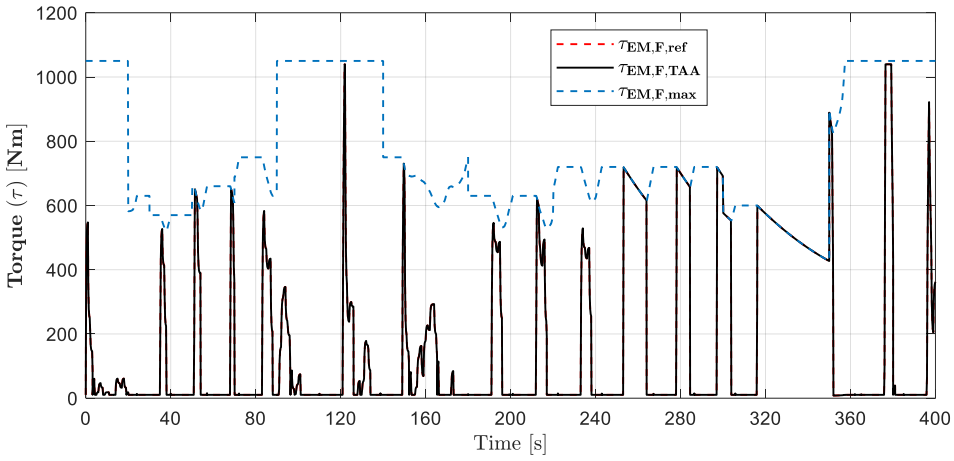

Figure 4-55: Front EM torque (TAA OFF)-reference torque (red), moderated torque (black) and max available torque(blue)

According to Figure 4-56, the reference velocity in this scenario is well tracked before the rear EM shutdown. However again the risk of failure should be noted due to overheating. Speed tracking for the inactive TAA case is still a bit better than the active TAA case (comparing Figure 4-53 and Figure 4-56 after t=250s accepting the failure risk to front EM). This is expected to be reflected in the critical metrics.

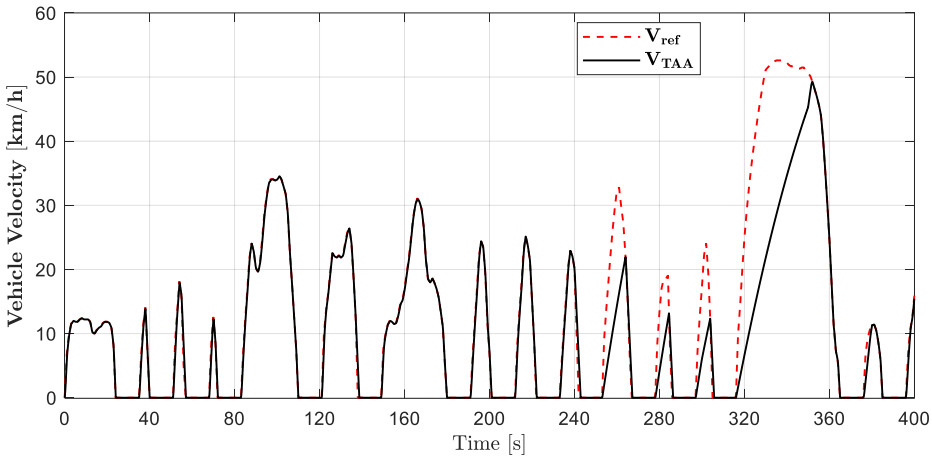

Figure 4-56: Vehicle velocity (TAA OFF)- reference velocity (red) moderated velocity (black)

4.4.3 Evaluation

To evaluate the TAA integrated flexible safe shutdown, a summary of the results in terms of critical metrics defined in D6.1 are given in Table 4-7. To calculate the overloading index (OI) for both EMs in this table, γ is set to 1.

Table 4-7: KPIs for critical metrics e-RT.

Test Case	Scenario	Mode	$OI_{EM,R}[\%]\ (\gamma = 1)$	$OI_{EM,F}[\%]\ (\gamma = 1)$	$\epsilon_{RMS}[km/h]$
1	S1FEMS1REM	TAA	0	0	0.84
	S1FEMS1REM	No-TAA	2	0	0.51
2	S1FEMS3REM	TAA	0	0	9.5
	S1FEMS3REM	No-TAA	2.9	29	6.6

It is clear from the table that activating the TAA reduces tracking performance as it is already expected and discussed in the simulation results analysis. However, it is clear that TAA does not allow EMs to work full-loaded in high temperatures. Although it is dependent on drive cycle, temperature profile, etc.; for the two scenarios simulated in this deliverable EMs go full-loaded. Specifically, in test case 2, the front EM works full-loaded in 29% of the time it is overheated.

The overloading index could be evaluated for different γs. Figure 4-57 shows this index for test case 1 and 2 scenarios. The overloading index in these scenarios, for the selected range of γ is zero when the TAA is active. It is seen from the figure that the EMs have to work almost full load (more than γ of full load) for up to 30% of the critical temperature period when the TAA is inactive.

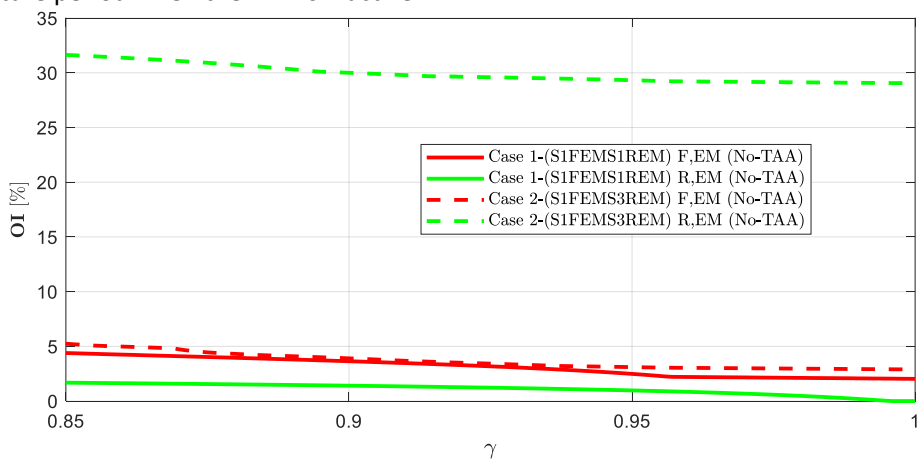

Figure 4-57: OI as a function of γ

The simulation results show that the EMs (and the battery if it faces a fault) never work with their maximum capacity in the critical temperature range, as required by manufacturer. This reduction in performance should be done with pre-alarm to the driver. Therefore, it reduces thermal stress and hence improves the safety and electric range. This can postpone or even remove possible shutdown risk due to more temperature rise. simulation results have shown that, the TA algorithm takes the necessary actions against communication faults as well. It is important to note that one of the main advantages of the proposed TA algorithm is being parametric and modular, so it can be easily implementable to any EV.

4.4.4 Conclusion

To be able to calculate the improvement with the systematic, and analytical approach; ASIL C is rated normally for the BMS SW [3], [4]. The assumption that the hard-ECU has a λ=6.10^{-6}. Hence, unavailability of the SW should not exceed the unavailability of the hard ECU, which is 6 . 10^{-7}[5]. For ASIL C, the reliability cost factor stated in *d*-COCOMO method is stated 'high' with a value of δ_H = 1.15. In this case study, the BMS SW is rated as ASIL D. Hence, the application of the systematic, analytical and objective software development approach during the complete lifecycle development will help achieving the safety goal, and reduce the ASIL rating as well as shown in Figure 4-58.

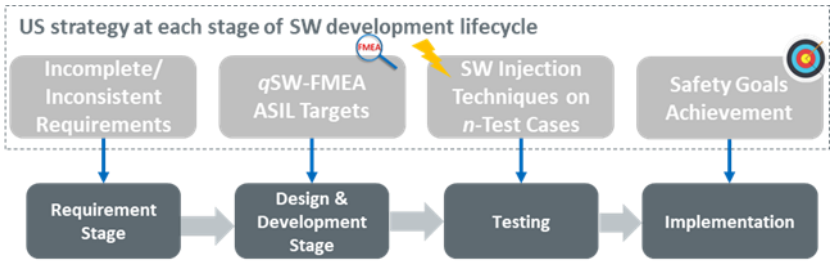

Figure 4-58: US strategy at each stage of development lifecycle

For an embedded SW listed with ASIL D, the reliability is "very high" corresponding to a value of δ_V = 1.40. Hence, the total reliability improvement using the approach can be re written as:

$$\Delta_\delta = \left(\frac{\delta_V - \delta_H}{\delta_V}\right) = \left(\frac{1.40 - 1.15}{1.40}\right).100\% = 17.8\% \qquad \textbf{Equation 1}$$

where, δ_V and δ_H are the reliability factor for very high and high reliability of the safety critical embedded software and, Δ_δ is the improvement of the reliability in percentage.

It can be noted that up to 1.18% in the reliability ranking can be possible when deploying tools such as the p-diagram or boundary-fault tree diagram.

In conclusion, to calculate the safety improvement of the proposed fault tolerant algorithm the analysis is done based on the reduction of the number of failures. Considering the fact that the failure rate (λ) of an AC polyphase is 10 failures/million hours during normal use of the EM [6]. Results of a survey on failures distribution in EMs, shows that nearly 17% of fails are initiated from overheating (Table 4-8). Therefore, 17 failures/ten million hours from overheating could be avoided by the TAA.

Table 4-8 No. of EM failures for outdoor applications [7]

Failure Initiator	No. of Failures	Percent
Transient overvoltage	2	2.2
Overheating	**15**	**16.7**
Other insulation breakdown	16	17.8
Mechanical breakage	26	28.9
Electrical fault/malfunction	9	10.0

Stalled motor	1	1.1
Other	21	23.3
Total	**90**	**100**

Accordingly,

$$\Delta_S = \left(\frac{\lambda_T - \lambda_{TAA}}{\lambda_T}\right) = \left(\frac{10.10^{-6} - 83.10^{-7}}{10.10^{-6}}\right).100\% = 16.7\% \qquad \textbf{Equation 2}$$

where, λ_T and λ_{TAA} are the failure rate of the traditional approach and the estimated failure rate of the TAA whereas, Δ_S is the possible improvement of the safety. It should be noted that there are other failures that initiate from other sources, but high temperature contributes to final failures. Since it is assumed that the TAA is removing overheating, therefore it can mitigate the severity in these cases as well. In other words, the TAA could remove the failures as the high temperature is the contributor in them, not the initiator. From this point of view based on the literature, the proposed algorithm even have the potential to improve the safety more than given in Eqn. 1, i.e. around 38% [8].

5 Project Objective Evaluation & Use Case Cluster Conclusion

The evaluation of each use case was shared in chapter 3 and this section is provided to conclude the overall results of the use case cluster 3. Battery safety from early design phase to product development and vehicle installation was studied throughout the use case cluster 3. Accurate battery models were developed to predict thermal runaway based failures in order to improve the battery safety at early design phases. Traction inverter induced AC current ripples studied at product development phase where batteries are built and ready for testing. At the last installation specific internal and external loads were investigated to define the potential safety improvements. Except for the battery, the vehicle control unit safety improvement was also studied. In order to quantify the improvement on safety following methods were proposed:

5.1 General considerations on safety

In the scope of Obelics project, safety is a term strongly related to the functional safety. This means in this context, that it is restricted to the functional and technical properties of the device. Any external safety measures (e.g. a housing covering the entire device) are not taken into account. We only take into account what the project aims to improve.

Generally speaking, the safety is regarded to consist of 3 major contributors, as was also already proposed in other studies on battery safety :

B = measure for the severity of an unwanted event
P = probability of occurrence of the unwanted event
C = Controllability of the event, once occurred, by the user

Then, the safety is calculated as

$$S = B \cdot P \cdot C \qquad (1)$$

In general, the overall safety is regarded as the effectivity of the combination of many contributing failure mechanisms in relation with potential harms. As a consequence, the way to improve the safety is to lower the factors B, P, C or to lower the number of contributing failure mechanisms. Both can be influenced in several ways.

5.2 Safety improvement in Obelics

In the Obelics project, as mentioned above, there were several project branches dealing with the safety improvement. The general philosophy here is that the influence on the safety is;

1) Executed by taking improving influence on the development (V-cycle) in several ways,
2) Evaluated by a comparison between the world before and after Obelics: what would improve, if the V-cycle is now equipped and improved by the newly developed methodologies?

Since the project deals with improvements on the technical performance and properties of the powertrain components, the factors B and C are out of the scope of Obelics and may be held constant. In this case, the safety improvement reduces to the question in how far the probability of occurrence of critical states P can be lowered in a new (imaginary) V-cycle executed under the help of the methods elaborated in Obelics.
The term “safety improvement” then reduces to the question: If there are X devices in the field, causing Y_{before} critical states: by which factor was Obelics able to reduce this number? This overall improvement factor I_{total} shall, as defined as a high level metric goal, take a value equal or higher than 10. It then reads:

$$I_{total} = \frac{Y_{before}}{Y_{after}} \geq 10 \qquad (2)$$

Generally speaking, the improvement factor and the percentage of improvement are connected via the following formula:

$$I\ (\text{in } \%) = 100 - 100/I \quad \text{or vice versa:} \quad I = 100\%/(100\% - I[\%]) \qquad (3)$$

The following table shows this dependency. It also makes clear that already seemingly low improvements by e.g. factor of 2 mean an improvement by 50%! On the other hand, it also shows that a further increase of the improvement factor leads to a smaller leap in percentage.

Table 5-1: Improvement given in % and numeric values and their interdependence

Improvement in %	Improvement factor I
20	1,25
40	1,66
50	2
70	3,33
80	5
90	10

5.3 Interpretation of the probability of occurrence P

As stated above, we have already derived that the safety improvement in Obelics is reached over influencing the V-cycle by means of several methods. These methods have a direct impact on the number of critical states in the field, and therefore are related directly to the safety and the improvement factor.
These methods were categorized as follows:

1. **Mechanistical approach/improvement of pre-knowledge**

Methods falling into this category deal with the technical improvement of the system on subcomponent, material and design properties. By introducing these methods into the V-cycle, this shall lead to a state where the probability of occurrence of a certain failure mechanism is lowered by structural improvement of the subsystem. Example: a simulation method on cell chemistry will lead to an improved ageing behavior of the battery and consequently the material-related origins of a thermal runaway will be lowered.

2. **Diagnosis functions**

Methods in this category aim to initiate an action as soon as a secondary mechanism related to the unwanted event exceeds a critical value. The diagnosis function therefore reduces the probability of occurrence in a different way than 1): The unwanted mechanism itself may take place, but the preceding action chain is broken. Example: a temperature monitoring of a cell will indicate an upcoming thermal runaway, and therefore the electrical connection will be interrupted as soon as the temperature exceeds a certain value. The thermal runaway is then abolished.

3. **Enabler**

The enabler is a term describing methods that in a more general way act on a wide range of the V-model. It is not dedicated to a specific failure mechanism, but acts in a certain way to all of them dealt with in the V-cycle. Example: probabilistic FMEA. This method influences the entire V-cycle by enabling the user to describe and estimate failures in a much more precise way than before.

In order to see which methods were elaborated in Obelics, and into which of the above categories they fall, a table was set up and handed to all partners involved in safety aspects. It was already described in the deliverable D5.6. In this table, also the category was asked for:

	How will the result enter the V-Model in **a new development** after Obelics?			
Method/Result	**Improvement of pre-knowledget**	**(online/onboard/in situ diagnosis or monitoring**	**"Enabler"**	**Others**
Please describe the method/result developed as a result of obelics. The wording must not necessarily correspond to the task description in the GA since the method dscription meant here is more menat as summary of what was done in the project.	*The Obelics result will enter the new develompment by an improvement of pre-knowledgeImprovement of State of the art. Please describe here in how far.*	*The obelics result will result in a monitoring/diagnosis feature minimizing the probability of the describe failure*	*The result will in general help to better estimate the overall effects quantitatively (example: probFMEA, new modelling technique, new experimental technique,...)*	*describe here if the result will not fall into one of the previous categories*

Figure 5-1: Excerpt on methods table sent to partners

An important statement is the fact that these methods act in a different way within the overall safety approach. This has to be taken into account in the procedure of assessing the entire safety improvement.

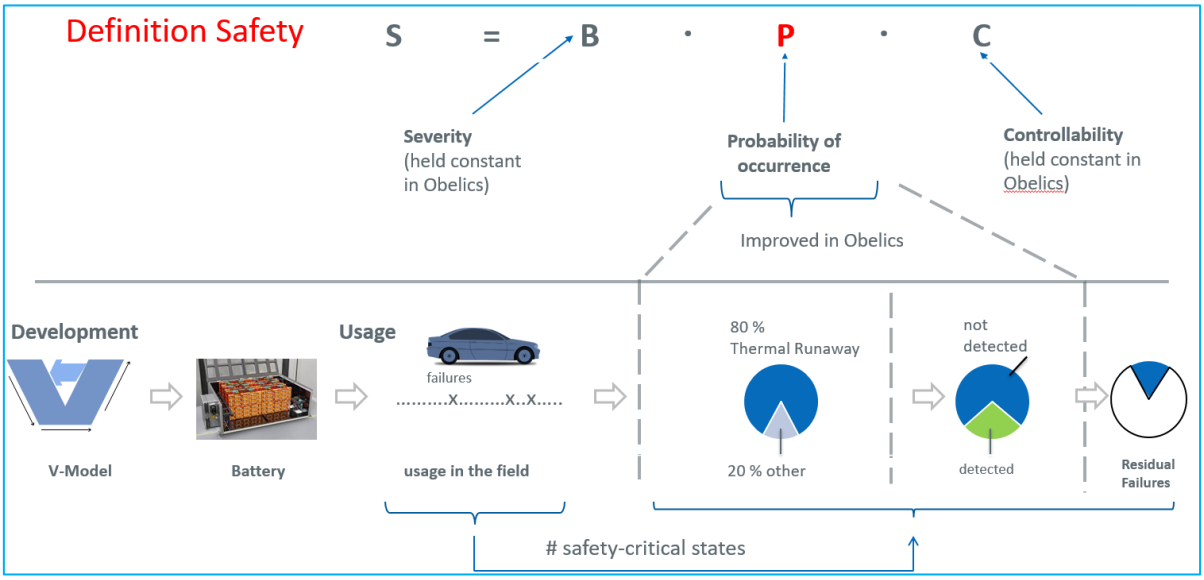

Figure 5-2: Definition of safety and situation in the field

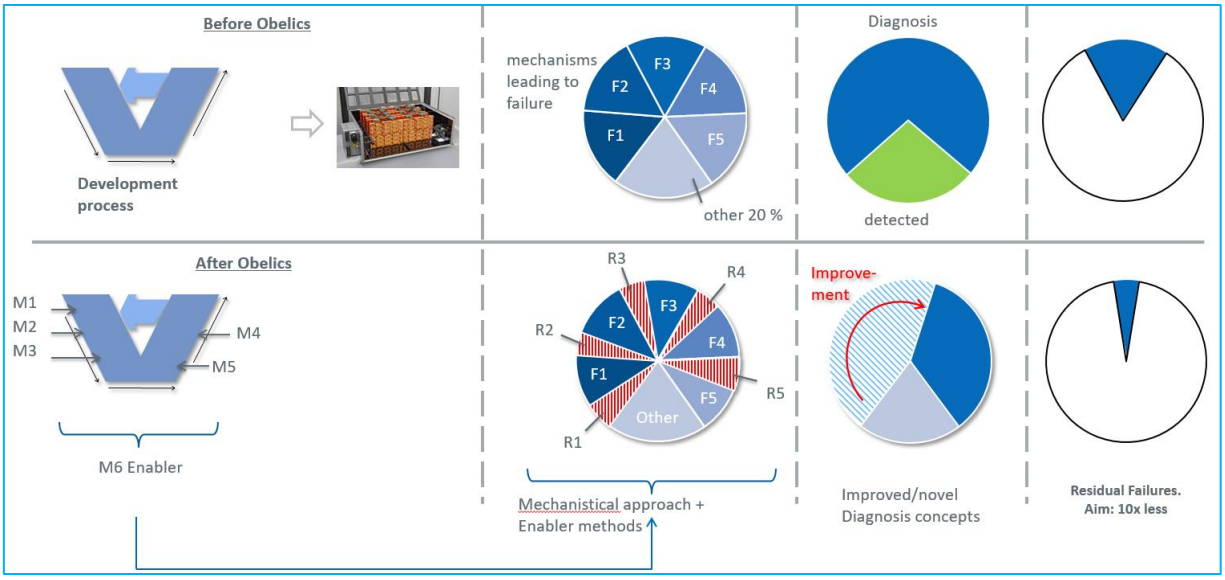

Figure 5-3 :Residual critical states before and after Obelics, indicating the overall safety improvement factor .

Figure 5-3 summarizes the philosophy of the assessment of the safety improvement. After Obelics, the imaginary V-cycle will be influenced by the results of the methods M_i developed in Obelics. These methods will reduce the amount of critical states in the field by an individual improvement factor I_i . This will result in a state where the fraction of failures assigned to this method F_i will be reduced by this factor, such that only a residual amount R_i of failures will be left:

$$R_i = F_i/I_i \qquad (4)$$

For sake of simplicity we assumed that if there were several methods addressing the same top level critical state, then this share of failures will be equally distributed along the overall failure scenario. The overall percentage share of a top level critical state in the overall amount of critical states was assigned capital letters A, B, C, …X. In our simplified example in the above figure, the event "thermal runaway" covers A% of all critical states, while "others" cover B, C, D… %.

The methods M1 … M5 in the above sketch represent methods falling into the mechanistic approaches. They lead to a direct reduction of critical states in the field. The method M6 is an enabler method acting on the entire V-cycle or at least on multiple damage mechanisms. It will contribute to a reduction of all failure fractions, and therefore the improvement factor multiplies with the mechanistic improvement factor. Also displayed in the figure a diagnosis function acting on a certain failure mechanism, in this case on mechanism A. This method leads to the situation that the residuals R1 ….n of all n Methods acting on mechanism A will further be reduced by its improvement factor. Therefore, this improvement factor enters the following equation as a multiplier.
Taking these considerations into account, the overall residual failures over all critical states A…X calculates as follows:

$$Rtot\ [\%] = \sum_{A,B,\ldots X} \left[\frac{A[\ share\ in\ \%]}{n\ (\#Methods)} \cdot \frac{1}{\prod I_{Diag,A} \cdot \prod I_{Enabler}} \cdot \sum_{i=1}^{n} \frac{1}{I_{[mechanism\ A],i}} \right] \qquad (5)$$

With

A…X:	%-share of the critical states resulting from top-level scenario A…X
n:	number of mechanistical methods applied to this scenario
$\prod I_{Diag,A}$	Product of all Improvement factors of diagnosis methods acting on the respective top level scenario
$\prod I_{Enabler}$	Product of all enabler improvement factors (no index since it acts on all methods)
$I_{mechanism\ A,\ i}$	Improvement factors of mechanistical Methods i…n acting on the respective share of failure states of top –level scenario A.

After calculating the residual failures with the above equation, the total improvement factor can be calculated as follows:

$$I_{tot} = 100\% / R_{tot} \qquad (6)$$

The individual improvement factors per method were also asked from the partners in the above-mentioned table. These improvement factors are best-guess-assumptions based on the expert experience in the respective field.

5.4 Assessment of battery safety improvement in OBELICS

The following show all methods elaborated in OBELICS in UCC3 and WP5 targeting the safety of the battery. The information shown there was condensed down from the tables shown in the Appendix of this document. In the "Method" column is a short description of the method, including a classification of mechanistic (M) or diagnosis (D). The enabler methods (E) are not listed there since these act on all mechanisms simultaneously. They are shown underneath the table and are represented in the columns E1 and E2, respectively. The blueish colored columns show the individual improvement factors as given/estimated by partners on the basis described in the

tables in the appendix. The top level scenario column shows the two major top-level scenarios treated in the project: The thermal runaway and the breaking of inner mechanical parts of the battery assembly. The column A [%] shows the share of the top-level scenario in the overall failure scenario. Due to the fact that no reliable source was found giving evidence for the real-world distribution between these failure events, their percentage shares were estimated as 80% and 20%. From expert judgement, this assumption appears reasonable. These values serve as a weighting factor, having the effect of laying an emphasis on methods aiming for lowering the risk of a thermal runaway.

Methods treated in UCC3 are highlighted in greenish background. In case a partner has given the improvement factors in percentage, this is given in brackets behind the factor.

Table 5-2: Safety evaluation of the battery, displaying methods in WP5 and UCC3.

Method	**Partner**	**M_i**	**D1**	**D2**	**E1**	**E2**	**Top-level scenario**	**A [%]**	**Resi-dual R_i [%]**
		Improvement factors I (partner estimation)							**Eq. 5**
M1 Virtual reliability assessment of batteries by means of coupled electrochemical, thermal and degradation models	UL	2	20 (95%)	3	1,5	1,05 (5%)	Thermal runaway	80	0,64 %
M2 Systematic, and analytical software development process **(UC3.4)**	US&FO	1,2 (17,8)							
M3 Optimized models for battery	VUB	1,05 (5%)							
M4 High frequency testing **(UC 3.2)**	AVL	1,33 (25%)							
(D1) Onboard Impedance spectroscopy of a Li-ion cell (monitoring concept), EIS and calibrated cell electrical model. **(UC 3.1)**	CEA	n/a							
(D2) Modelling of impedance spectroscopy	NIC	n/a							
M1 Experimental analysis of vibrational loads on cell pack level **(UC 3.3)**	Bosch	1,5	1,5	n/a			Break of inner parts	20	5,17 %
M2 Experimental analysis of vibrational loads on cell level/Eigenmode analysis	AVL	1,8							
(D1) Virtual treatment of vibrational loads	Bosch	n/a							
E1 = probabilistic FMEA (LBF) E2 = Assessment of functional safety of battery (VUB)							**Overall sum**	R_{tot}	5,81 %
							Improve-ment factor (Eq. 6)	I_{tot}	**17**

This calculation gives a first orientation on the impact of the applied methods. The procedure of deriving the input figures from partners and the calculation scheme itself contain several simplifications and assumptions in order

make this assessment possible. Therefore the values gained from it underlie an uncertainty, leading to the fact that the values given will have a certain scatter band. However, it may still serve for a first rough orientation.

As can be seen from the table, the application of all elaborated safety-oriented methods will lead to a calculated **safety improvement by a factor of 17**.

Note: The method of calculating the safety improvement was elaborated particularly for this project in order to allow a rough estimation of the expected impact of these methods on safety. It does not replace a standard-based safety assessment of a concrete product.

6 Appendix: Safety evaluation tables from WP5

In this appendix, the safety evaluation tables which are the basis for the above-mentioned safety analysis will be shown in full extent. These tables were already mentioned and their purpose was explained in D5.6. At that stage of the project, not all inputs from partner were completed, so here all tables are shown with all inputs. The tables contain the method-specific safety improvement factors as well as a short explanation how this factor was determined. Also, the tables contain summarized information regarding the methods itself with respect to their goals, their impact and there applicability. Moreover, the information regarding the entering stage of the V-cycle is given (see description above) laying the ground for the categorization of the methods.

Section 6.1 contains the tables for the battery safety methods. As can be seen, 3 of the 4 Use Cases already displayed here since these methods were elaborated in WP5. UC 3.2 was treated in UCC3 without interaction with WP5 and therefore was added to the above table 5-2 separately. Since only the battery safety methods are relevant for the battery safety assessment and for the assessment of the goal of safety improvement by a factor of 10, these methods from the table in section 6.1 were condensed into the above table 5-2.

Sections 6.2 and 6.3 display the contents for the inverter and for the e-machine/vehicle level, respectively.

6.1 Battery safety methods, information and assessment

Table 6-1: Methods for Battery safety part 1

Method/Result	Part-ner	Source	Top level safety scenario	what was investigated	Goal of investigation with respect to safety improvement	Affected components	How will the result enter the V-Model in a new development after Obelics? Improvement of pre-knowledget	(online/onboard/in situ diagnosis or monitoring	Enabler	How was the safety improvement factor determined?	Safety improvement (numerical or %)
Virtual reliability assessment of batteries by means of coupled electrochemical, thermal and degradation models	UL-Bat	WP5, WP2	Thermal Runaway	Initial links in the chain of reactions leading to the TR, i.e. highly exothermic reactions of SEI decomposition and reaction between intercalated Li and electrolyte. Heat sources due to Li-exchange between primary particles. Heat sources due to production injected deviations during cell manufacturing.	Study was aimed towards investigation how elevated temperaures affect chemical (SEI decomposition) and electro-chemical reactions (Li-electrolyte) within the cell and subsequent heat losses that additionaly increase cell temperature. Additionally, study was performed how deviations within the electrodes (uneven porosity and active material loading) during call manufacturing affect local heat dissipation.	Battery on the level of cathode/separator/anode cell sandwich.	Advanced virtual representation of the electrode was developed by considering agglomeration of primary particles. Additional heat sources in phase-separating materials due to Li-exchange between primary active particles were added to the established ones.	n/a	Plausible virtual representations of different materials. Implementation of various degradation mechanisms with higher fidelity offers improved predictability of outbreak of thermal runaway.	For poorly designed cooling systems or BMS's, the factor of improvement in safety can, therefore, be greater than 2, whereas for well-designed ones, it can be below 2. For overall factor estimation, value of 2 was thus chosen.	2
Experimental analysis of vibrational loads on cell pack level	Bosch LBF	WP5, UC3.3	break of inner mechanical parts and fixing parts	The vibrational loads were determined by a teast road driving campaign.The loads were applied vya MAST Test stand at LBF. Transfer funtions from the fixing points to dedicated mechanical parts in the interior were determined and evaluated	The aim was to 1) compare the internal loads to existing standards in oder to derive conclusions for future test procedures, 2) to evaluate the influence of T and SoC on vibrational loads, 3) to estmate the effect and neccesity of possible monitoring concepts targeting the mechanical loads inside the battery	a) cell pack housing, fixing ribbons b) same as a)	Improvement by pre-knowledge, that the loads are not valstly affected by the SoC and T. Mechanical parts can be designed according to the determined loads and the uncertainty regarding their durability is minimized	n/a	n/a	reduction of operational loads leads to a decrease in failure probability. Value is estimated Best guess estimation from experience and expert knowledge	1,5
Virtual treatment of vibrational loads, vehicle dynamics	Bosch	WP5	break of inner mechanical parts and fixing parts	A variaty of data based models were investigated to describe the vibration transfer path.	(1) Virtual assessment of loadings to the battery by using variable street surface configurations (2) Online damage estimation	a) cell pack housing, fixing ribbons b) same as a)	Wider knowledge of the mechanical loading situation of the battery in the vehicle Knowledge about simulation models to describe vibration transfer behavior in a vehicle	online/onboard diagnosis possible. The results proof that a predictive maintaince strategy with such simple models can lead to increase safety.	n/a	Best guess estimation from experience and expert knowledge	1,5
High frequency testing	AVL	WP4, UC3.2	Thermal runaway	Increased power losses leading to excessive heating and thermal runaway. Failure of BMS due to EMI. A new test rig was designed to realize field relevant electric switching frequencies. That means the battery system can now be tested with field relevant electric load conditions which are more criticial compared to the current test rigs.	Create new test rig and put relevant electric loads to the battery.	cells, bus bars, cell interconnects/welding points, BMS	higher bandwidth of AC currents that can be superimposed to the DC charging / discharging current. The new function will help to challange the battery and find weak operational points.	impedance measurement of each cell posssible	n/a	Increase of losses due to skin effect in a copper conductor of 95 mm^2 caused by a ripple current at 20 kHz with magnitude 20% (RMS) of DC current: +25% E.g. Tesla Model 3: 30 kW to 37.5 kW -> 7.5 kW extra heat load for cooling system.	25%
Experimental analysis of vibrational loads on cell level/Eigenmode analysis	AVL	WP5	break of modul terminals or modules	Eigenmode analysis with modules mounted or without.	Mechanical load transfer from battery pack system to modules.	Modules	Increased knowledge on the mechanical load transfer from Pack to module. Better tuned simulation models.	n/a	The result will help to take into account the damping factors of modules in the simulation.	Potentially damaging responses are in a high frequency range, usually not reached through road excitation (< 200Hz). Estimation as done by comparison of load reduction with S/N curves of used materials	1,8

Table 6-2: Methods for Battery safety part 2

Battery	**Onboard Impedance spectroscopy of a Li-ion cell (monitoring concept), EIS and calibrated cell electrical model.**	CEA	WP5, WP6, UC3.1	thermal runaway	All along the tests, the electrochemical impedance is recorded with the embedded electronics. Comparisosn between the results obtained from the two techniques should give predictive information. the impedance will be traced on Nyquist plots and we will determine and trace over time some points of those Nyquists in order to get meaningful information from them.	The aim is to stop using a cell or the whole battery if a dangerous state is up to come, or if its probability of occurrence becomes seriously high. Passenger information for safety is also recommended.	Battery single cells, goup of cells or the whole battery, including the BMS (Master and Slaves parts).	n/a	Impedance spectroscopy could be integrated in future Smart Cell designs. The technique will allow the use of cells that have not been fully tested at each possible state, as the electrochemical impedance espectroscopy will allow the BMS of the vehicle to predict the states in real time, thus saving test time and improving safety.	n/a	Literature and own knowledge based assumptions: we can suppose that 95% of cell failures due to overheating are detected. In most cases (60%) stopping the vehicle and disconnecting the whole battery from the the motor inverter, the charger and/or every single DCDC converter can prevent the battery and the vehicle from burning.	**95%**
	Optimized models for battery	VUB	WP5, WP2	Thermal runaway	The 1D electrothermal model, developed in WP2, have been optimized for the assessment of functional safety and failure mechanism prediction.	Improved electrical and thermal models of the battery allow optimized control of the operational conditions to ensure maximum safety and reliability of the system.	a) Battery system, b) BMS	n/a	These kinds of models have been optimized to simulate temperatures in the defined points without considering too much details which makes it suitable for real-time simulations.	n/a	Baseline failure probability based on historical commercial data. 5% improvement estimated due to improved electrical and thermal models for BMS applications	**5%**
	Assessment of fuctional safety of battery	VUB	WP5	Thermal runaway	Experimental assessment of hot-spots on the cell surface at high c-rates	A reduced order thermal model was developed which is able to simulate both air-cooling within the battery pack and thermal conduction between individual cells at acceptable computational effort. The developed method for thermal model order reduction and innovative thermal parametrization techniques in the frequency domain within the Obelics project will increase the accuracy and reliability of future battery system models and enhance future development of electrified powertrains.	a) Battery system, b) BMS/thermal management system	n/a	The assessment allows insights into the optimal placement of temperature sensors within the battery module.	n/a	Baseline failure probability based on historical commercial data. 5% improvement estimated due to improved electrical and thermal models for BMS applications	**5%**
	Systematic, and analytical software development process	US	WP5, UC3.4	Thermal runaway. Irregularity in battery operation, overvoltage, overcurrent, cell unbalance	Causes of SW failures	To reduce the software failures for the energy management algorithm of (soft-ECU) at the early design phase due to the: i) Incomplete/Incosistent Requirements ii) shortcoming of traditiol FMEA (subjectivity and bias) that would affect	a) Battery Management System (BMS), b) Battery System	Increased visibility,more accurate calculation of the RPN values, better prediction of the failures. Mitigation of failure at early design phase, selection among alternative risk mitigation solutions, to further improve the BMS software functional quality, and reduces the possibility of irregular battery operation.	n/a	Mitigation of failure at early design phase, selection among alternative risk mitigation solutions, to further improve the BMS software functional quality, and reduces the possibility of irregular battery operation.	Based on algorithmic approach used for estimating the safety-critical embedded software effort. By following the systematic, and analytical approach during the BMS software development phase, will enhance the safety of the battery system by reducing the failures which can causes irregularities in the operation	**17,8%**
	Impedance spectroscopy (theoretical and modelling)	NIC	WP5	thermal runaway	Systematic studies of correlation between battery capacity, internal resistance and impedance (EIS) response during long-term cycling of commercial cells. Advanced experiments on laboratory-build cells were performed where variation of electrolyte salt concentration was employed.	The 3 main goals were: 1) experimental verification of existance of direct correlation between evolution of battery capacity and evolution of EIS; 2) development of novel advanced physical-based transmittion-line model of cathode; 3) finding relation between EIS and microscopic changes in particles of active cathode material.	1) a) battery cell, b) the same; 2) a) cathode, separator, electrolyte, Li metal anode b) cathode, separator, electrolyte; 3) a) cathode active material b) the same	EIS can be used for tracking battery cell degradation: i) New combination of experimental techniques to follow battery degradation. ii) Advanced EIS model	n/a	n/a	Best guess estimation from experience and expert knowledge	**3**

6.2 Inverter safety methods, information and assessment

Table 6-3: Methods for Inverter safety

Inverter	**Optimized models for inverter**	VUB	WP5	Overheating, overall breakdown by electrical limit derating.	Losses and heating for new WBG technology switches. Electro-thermal performance and derating.	Performance over the wide operation range of the component with respect to losses thermal load and derating of components. Cooling impact. Optimized control for safe and reliable operation.	a) inverter	Accurate modeling and verification for WBG inverters. Model parameters/sensitivity and realistic load profile consideration. Better designs and control during operation, with proper cooling and derating depending on operation.	n/a	n/a	Baseline failure probability based on IGBT based inverter data using Coffin-Manson equation. 1.15% improvement estimated due to improved thermal stress properties in the SiC MOSFET power module.	15%
	Assessment of FuSa of Inverter	VUB	WP5	Overheating, thermo-mechanical failure.	Modeling of thermal related risks and degradation with realistic vehicle load profiles.	Thermal stress and degradation of the component with derating impact on voltage, current, power, operating conditions.	a) inverter	Derating needs and breakdown assessment for real driving profiles.	n/a	n/a	Best guess estimation from experience and expert knowledge	1,2
	Experimental setup for HF Inverter, B2B Tests	AVL	WP4, UC3.2	on Load: - phase cut off (open phase) - short circuit phase to phase - short circuit phase to DC+ - short circuit phase to DC- - Temperature rise test - load dump - HV voltage cycle - active/passive discharge - Behavior in the event of a crash	- special test setups needed for the tests (load dump + active discharge) - the Behavior of the inverter at different scenarios and events	- jump to the Safe State is required in case of phase short circuit or cut off (ACS or freewheeling) - the purpose of the Temperature rise test is to ensure that the thermal performance of the inverter is as designed - the load dump test verifies if the Inverter is able to limit an overvoltage caused by a load dump. - HV voltage cycle to check the component's HV-voltage-dependent serviceability and performance. - The discharge process to a voltage under 60 V, starting from Vopmax HV, must be completed within the td,a time specified in the Component Performance Specification	Inverter as a System Inverter internal components	The HV-Safety tests can be tested and evaluated more in detail before the origin e-machine is available. In the earlier development phase and an higher efficiency of the test coverage - concentrated on the power electronic - will be possible under realistic high electrical power load. Earlier testing under realistic load. Together with Software integration tests. Frontloading of test coverage.	n/a	n/a	Best guess estimation from experience and expert knowledge	1,5
	Road tests "SimRod inverter+motor+battery"	SIE	WP4	thermal runaway (battery) / isolaton degradation (motor) / unknown (inverter)	The SimRod was driven around the 'Leuven Drive Cycle' (in ECO mode, and in SPORT mode), measuring electrical powers (DC / AC), battery temperatures, inverter heatsink temperature, motor temperature (stator winding)	No original goal wrt safety improvement. However, the data shows clearly that the motor heats up (fairly quickly) at higher speeds. Possibly a similar statement can be made wrt the battery temperature, although it remained below 30°C all the time, I believe.	battery cells, motor, inverter	verification of prototype (according to SOTA) + validation of XiL (model) behaviour (in view of useful XiL testing)	n/a	n/a	using calibrated battery models + XiL-based information on the effect on DC current consumption due to altered design, the expected battery temperature could be kept lower / (DC) current limiting could be done more effectively	1,9
	XiL tests "SimRod inverter+motor"	SIE	WP4	Isolaton degradation (motor) / unknown (inverter)	A part of the operational test (LDC) was replicated on the XiL rig (only speeds < +- 70 kph, i.e. 5000 rpm) in which the inverter and motor are the real components. Electrical and mechanical powers were measured, along with motor and inverter temperatures. Also model variables are captured (e.g. covered speed, road slope vs time, ...)	No original goal wrt safety improvement. However, the data shows clearly that the motor heats up (fairly quickly) at higher speeds.	motor, inverter	On the XiL rig, we can do additional parameter sensitivity analyses which are not feasible in reality. E.g. what is the effect of an altered gearbox ratio (on motor temperature) / what is the effect of an altered DC voltage level (on E-powertrain efficiency)?	n/a	n/a	using calibrated inverter / motor models + XiL-based information on the effect of design alterations on motor/inverter temperature, motor/inverter overheating risks can be reduced. Factor 10 is valid for induction motor.	10

6.3 E-machine and system level safety methods, information and assessment

Table 6-4: Methods for e-machine and vehicle safety

E-Machine	**Virtual reliability assessment of E-motors by using scalable and multi-physically integrated models**	UL-E	WP2, WP3	Unexpected temperature rise	Thermal profile of electrical machine during usual and unusual conditions	Winding insulation lifetime prediction and preventing, demagnetisation prediction and preventing	a,)winding, magnets, cooling system; b,) winding, magnets	Thermal model generation, insulation lifetime model generation, demagnetization detection and prediction. The results helps to improve online/onboard monitoring and diagnostics	Regular service monitoring and tests, onboard measuremets of induced voltage (backEMF), onboard temperature monitoring and modeling winding lifetime estimation	n/a	Best guess estimation from experience and expert knowledge	9
Vehicle level	**HAZOP analysis of braking system**	Unifi	WP5	Primary: Regenerative and/or hydraulic brake unavailability Secondary: ABS and/or ESP controller unavailability	Considering the brake-by-wire system layout of the reference EV UC (component, rendundancy, controller, etc.), and related failure rate/distribution, a virtual simulation scenario is implemented with a model-based approach, in order to asses the effect on the vehicle behaviour throught an Hazard and Operability Analysis (HazOp)	In relation to ISO26262 standart, we evaluate the actual and target ASIL (Automotive Safety Integrity Level) relatively to the investigated brake funcionalities. Then, modification of the by-wire plant are proposed (replacment of component, redundancy of signals), along with the synthesis of specific control strategy which can avoid/handle dangerous situation and ensure brake-by-wire reliability		Respect to the actual SoA, the current activities propose the definition of a systematic methodology based on model-based HazOp approach and ISO 26262 standard specification, in order to: evaluate and asses the actual and target Automotive SIL; establish plant modification and control strategy to fit the previosly established safety requirment.	n/a	n/a	SoA and literature investigation, component and system data-sheet, simulation activities (improvement factor estimated by LBF on best guess basis)	1,7
	Software	US	WP5	Irregularities in software operation and failures	Causes of SW failures	To reduce the software failures for the energy management algorithm of (soft-ECU) at the early design phase due to the: i) Incomplete/Incosistent Requirements ii) shortcoming of traditiol FMEA (subjectivity and bias) that would affect	Powertrain components and related vehicle operations	Increased visibility,more accurate calculation of the RPN values, along with better prediction of the failures with addition of the scope visibility.	n/a	n/a	Using the mathematical approach for effort calculation of the ECU software that is compitable with ASIL D. Following the systematic, and analytical approach during the Energy Management software development phase, will enhance the safety by reducing the failures which can causes irregularities in the operation	17,8%
	Virtual Assessment of Functional Safety of All Wheel Drive e-RT: Energy Management Strategy with Integrated Safety Module against Electrical Machine Thermal Faults	US	WP5	EM failures, temperature rise	Torque moderation in single motor configuration	To mitigate the EM temperature rise	Electrical Machine: Traction/braking operation	Development of a fail safe energy managment algorithm that modulates the EM torque with respect to increase in temperature considering its effects on the EM performance	n/a	n/a	The system designed for the SM configuration is a fail-safe system, in which the EM on the basis of temp fault will lead to a shutdown in a controlled and safe manner. Hence the TM algorithm will reduce the failures making the EM operations more safer.	16,7%
		US	WP5	EM failures, temperature rise	Torque allocation and compensation in all wheel drive	To mitigate the EM temperature rise. Mitigation of the abrupt temp rise leading to interruption/permanent malfunction of the EMs operation. Bringing the vehicle to a safe state if any temperature faults occurs and continue to track the desired speed profile	Electrical Machine: Traction/braking operation	Fault tolerant energy managment algorithm development that can allocate or compensate required torque using hardware redundancy in case of abrupt temperature rises in traction motors	n/a	n/a	he system is both fault tolerant and fail safe. i) Fault tolerant: Due to the hardware redundancy, the temp faults in any EM wil lead to torque allocation via which the overall system can tolerate the fault ii) Failsafe: Due to temperature fault in both EMs at the same time or comm error in same time, the system will shutdown in a controlled and safe manner The TAA along with torque compensation mechanism will reduce the temp faults making EM operations more safer	16,7%
	probFMEA	LBF	WP5	does not affect, does describe and connect failures	Application of probFMEA to powertrain, implementation into development cycle, integration of nuerical investigation	improvement of V cycle frontloading due to efficient implementation of the method.	all componens displaied in the failure net	n/a	n/a	Clearly an enabler method: supports the accurate and efficient treatment of the descending branch of the V model, acts on system level.	Method woill influence the accuracy and quality of all safety-related steps in the V-cycle. The improvement factor is an estimation that multiples to all other factors.	1,5
	Methodology definition foreploitation of vehicles system models from WP3	SIE-SAS	WP5, WP3, WP2	Transistor Diode Module disconnection Transistor Diode Short circuit module	dedicated inverter component to an analysis such failure in reasonable CPU time	the objective is to offer inverter component allowing fast and consistent failure mode to test all potential failure and study their impact on vehicle level	inverter models	increase control calibration robustness by virtually checking all different inverter failure modes at component and vehicle level	n/a	n/a	Method is able to filter out multiple failures during development from different subsystems	2

7 Risk Register

7.1 Risk register

Mention here the risks that are linked to this deliverable. See the list of risks on the OBELICS sharepoint:
https://projects.avl.com/16/0142/Documents/02_Deliverables/OBELICS_Deliverables%20list-TIMELINE_27092017.xlsx?Web=1

If a new risk occurred, please introduce in the table below, and mention;

"With reference to the critical risks and mitigation actions this deliverable is not linked to any open risk. See the monitoring file of the WPLB
https://projects.avl.com/16/0142/Documents/02_Deliverables/OBELICS_Deliverables%20list-TIMELINE_27092017.xlsx?Web=1

During Deliverable 6.3 no further risks were identified.

8 References

[1] 2016 Automotive Warranty & Recall Report: Industry Insights for the Road Ahead," SRS: Stout Risius Ross, 2016.

[2] Pries, Kim H. Failure mode & effects analysis in software development. No. 982816. SAE Technical Paper, 1998.

[3] Vestin, K., 2015. N-BMSs, A Novel ISO-26262 Compliant Battery Management System.

[4]Lithum Balance Co. 2019, Functional Safety Requirements

[5] Hu, Z., Zhang, F. and Wei, Z., 2016. Research on Fault Tolerant Strategy and Reliability of Steering-by-Wire. International Journal of Modeling and Optimization, 6(2), pp.106-109)

[6] Tyrone, L. and Jones, T., 2011. Handbook of reliability prediction procedures for mechanical equipment. In Naval Surface Warfare Center West Bethesda. NSWC-11.

[7] O'DONNELL, P., Heising, C., Singh, C. and Wells, S.J., 1987. Report of large motor reliability survey of industrial and commercial installations. III. IEEE Transactions on Industry Applications, 23(1), pp.153-158.

[8] Sin, M.L., Soong, W.L. and Ertugrul, N., 2003, October. Induction machine on-line condition monitoring and fault diagnosis-a survey. In Australasian universities power engineering conference (Vol. 28, pp. 1-6).

[9] Kotub Uddin, Andrew D. Moore, Anup Barai, James Marco, "The effects of high frequency current ripple on electric vehicle battery performance", in Applied Energy, Volume 178, 2016, Pages 142-154, ISSN 0306-2619, https://doi.org/10.1016/j.apenergy.2016.06.033.a

[10] M. J. Brand, M. H. Hofmann, S. S. Schuster, P. Keil and A. Jossen, "The Influence of Current Ripples on the Lifetime of Lithium-Ion Batteries," in IEEE Transactions on Vehicular Technology, vol. 67, no. 11, pp. 10438-10445, Nov. 2018, doi: 10.1109/TVT.2018.2869982.

[11] M. Schlüter, M. Gentejohann and S. Dieckerhoff, "Impedance Analysis of an Automotive DC Bus," 2020 22nd European Conference on Power Electronics and Applications (EPE'20 ECCE Europe), Lyon, France, 2020, pp. P.1-P.10, doi: 10.23919/EPE20ECCEEurope43536.2020.9215803.

[12] C. Rettner, G. Jacob, M. Schiedermeier, A. Apelsmeier and M. März, "Voltage ripple analysis based on DC-link current harmonics for Voltage Source Inverters," 2019 20th Workshop on Control and Modeling for Power Electronics (COMPEL), Toronto, ON, Canada, 2019, pp. 1-6, doi: 10.1109/COMPEL.2019.8769623.

[13] Xuning Feng, Minggao Ouyang, Xiang Liu, Languang Lu, Yong Xia, Xiangming He, Thermal runaway mechanism of lithium ion battery for electric vehicles: A review, Energy Storage Materials, Volume 10, 2018, Pages 246-267

9 Acknowledgement

The author(s) would like to thank the partners in the project for their valuable comments on previous drafts and for performing the review.

Project partners:

Partner no.	Partner organisation name	Short Name
1	AVL List GmbH	AVL
2	Centro Richerche Fiat SCpA	CRF
3	FORD Otomotiv Sanayi Anonim Sirketi	FO
4	Renault Trucks SAS	RT-SAS
5	AVL Software and Functions GmbH	AVL-SFR
6	Robert Bosch GmbH	Bosch
7	SIEMENS INDUSTRY SOFTWARE NV	SIE-NV
8	SIEMENS Industry Software SAS	SIE-SAS
9	Uniresearch BV	UNR
10	Valeo Equipements Electroniques Moteurs	Valeo
11	Commissariat à l'Energie Atomique et aux Energies Alternatives	CEA
12	LBF Fraunhofer	FhG-LBF
13	FH Joanneum Gesellschaft M.B.H.	FHJ
14	National Institute of Chemistry	NIC
15	University Ljubljana	UL
16	University Florence	UNIFI
17	University of Surrey	US
18	Das Virtuelle Fahrzeug Forschungsgesellschaft mbH	VIF
19	Vrije Universiteit Brussel	VUB

This project has received funding from the European Union's Horizon 2020 research and innovation programme under grant agreement No 769506.